*J. Fluid Mech.* (1993), *vol.* 251, *pp.* 627–660



# On longitudinal vortices in curved channel flow

By ALESSANDRO BOTTARO
IMHEF-DME, Ecole Polytechnique Fédérale de Lausanne, CH-1015 Lausanne, Switzerland

(Received 7 July 1992)

The laminar flow in a curved channel is studied numerically to analyse the initial formation, development and interaction phenomena of an array of centrifugally induced longitudinal vortices arranged across the span of the channel. Simulations employing streamwise periodic boundary conditions (*temporal model*) as well as inlet–outlet conditions (*spatial model*) are carried out. In the temporal approach the interactions (pairing of vortices and growth of new vortex pairs) of fully developed vortex pairs are time-dependent, whereas in the spatial approach these events are inherently steady and concern vortices not in their fully developed state. The initial spatial development of the vortices is in excellent agreement with results of a linear stability analysis up to fairly large disturbance amplitudes. In the nonlinear regime a good agreement with experimental results has also been found. The receptivity of the flow is very important in a convectively unstable situation such as the present one and different behaviour is found at fixed Reynolds number (equal to 2.43 times the critical value for the onset of Dean vortices): the flow can be either steady or undergo a continuous sequence of merging and splitting events, depending on the inlet conditions. In the latter situation decorrelated patterns of low- and high-speed streaks are produced in streamwise–spanwise planes and they bear several similarities to near-wall coherent structures of turbulent boundary layers.

## 1. Introduction

The flow in curved channels and ducts has been, and still is, the object of intense investigations, because of its intrinsic interest, as well as its relevance to several technological and physical problems that involve curved passages and surfaces, such as turbine blades, airfoils, heat exchangers, river flows, etc. The problem is commonly known as the *Dean problem*, from the name of the first researcher to analyse it. Dean (1928) found that above a certain critical value of a dimensionless number, that became to be known as the Dean number and is an appropriate combination of a Reynolds number and a curvature parameter, two-dimensional, steady, longitudinal vortices develop on top of a basic Poiseuille-like flow state. These secondary flows, produced by an unstable stratification of angular momentum, are such that the flow spirals as it proceeds downstream. Secondary motions alter the wall stress distribution and heat transfer characteristics: as such, it is important to be able to understand and predict them.

If solid sidewalls are present in a curved duct, Ekman vortices, induced by the sidewalls, are produced at all values of the Reynolds number, $Re$. When curved ducts of small aspect ratio (ratio between the span and the channel height) are considered, the few Dean vortex pairs that appear in the cross-section of the duct above a threshold value of $Re$ interact with the Ekman vortices. The study of such interactions is beyond the scope of the present investigation. However, most work published on Dean vortices

deals with small- ($< 4$) aspect-ratio curved ducts. Thangam & Hur (1990) studied the problem through finite volume simulations for steady two-dimensional fully developed flow. They found that, typically, one pair of vortices is contained in the cross-section, but eventually at a certain critical Reynolds number a new vortex pair appears to 'pop' out of the outer wall. This is consistent with previous two-dimensional theoretical studies (Winters 1987) which indicated that four different solutions may exist: three symmetric solutions (two with two pairs of vortices and one with one pair) and an asymmetric one. The only study of spatially developing flow in a curved duct of small aspect ratio (equal to one) has been performed by Ravi Sankar, Nandakumar & Maslihay (1988). They performed finite volume simulations of the steady parabolized Navier–Stokes equations, to verify that 2- and 4-cell solutions appear. Interestingly, they found spatial streamwise oscillations which corresponded to the creation and annihilation of a small vortex pair near the outer wall (cf. their figure 6). Most of the literature relevant to the small-aspect-ratio case is contained in the papers cited above.

When the aspect ratio is large, several pairs of cells may coexist across the span of the cross-section. This case is most often studied by employing periodicity in the spanwise direction, but work by Finlay & Nandakumar (1990) has focused on the Ekman vortices induced by no-slip sidewalls and their interaction with the Dean vortices. Fully developed flow was considered, which means that the spatial development up to the parallel flow state was ignored. The first three-dimensional numerical work on a periodic array of Dean vortices arranged across the span was carried out by Finlay, Keller & Ferziger (1987, 1988). They performed calculations by a spectral technique in a channel with periodic boundary conditions in the spanwise and streamwise directions. In the spanwise direction only one pair of vortices was included. They adopted the so-called temporal model in which a source term, representing a pressure gradient, drives the flow, which is periodic in the streamwise direction. Even though temporally developing simulations may shed some light on the physical processes under consideration, the spatial development (from its linear inception on) is only mimicked. Furthermore, by considering a computational box with only one pair of vortices, vortex interaction mechanisms cannot be properly represented.

Recently, Bottaro, Matsson & Alfredsson (1991) and Matsson, Bottaro & Alfredsson (1991) have provided some comparisons between experiments and numerics on the spatial development of the flow in a curved channel of large aspect ratio. The adoption of a large aspect ratio is important because experiments (Ligrani & Niver 1988; Matsson & Alfredsson 1990, 1992) have shown that complex vortex interactions may occur, resulting in the creation and cancellation of vortex pairs, with consequent modification of wavelengths. These mechanisms are likely to play a very important role in the transition process, and as such deserve a study in themselves. The problem of interaction of vortex pairs has been studied theoretically by Guo & Finlay (1991). They performed a linear analysis of the stability of axisymmetric vortices to spanwise-periodic perturbations and reported that in curved channel flow there is a so-called *generalized Eckhaus stability boundary*. It is a closed curve contained inside and tangent, at the critical point, to the linear stability curve for the onset of Dean vortices in the wavenumber/$Re$ plane. Outside of this closed curve the flow is unstable to spanwise disturbances. The critical point defines $Re_c$, the critical Reynolds number for the onset of Dean vortices. Above $Re/Re_c = 1.7$ a system of infinite spanwise length is always unstable to spanwise perturbations. If the spanwise wavenumber is too large two vortex pairs will merge to form one pair, and the wavenumber will be reduced. If it is too small, a new pair of vortices will form between two existing pairs, causing the

wavenumber to increase. Such events are defined as merging and splitting of vortices. It is clear that the Eckhaus instability is of fundamental importance in the wavenumber selection process.

Merging and splitting events occur in a variety of circumstances. They have been noticed to occur in Görtler vortices (Bippes 1978; T. Maxworthy 1990, personal communication), as well as in plane rotating channel flow (Yang & Kim 1991; Alfredsson & Persson 1989). Mutabazi *et al.* (1990) report *defects* in the Taylor–Dean system, corresponding to rolls that undergo splitting events. These defects are found to be responsible for a decorrelation of patterns and as such they represent an ideal model on which to test turbulence theories. Mergings of spanwise vortices have been recently described in impulsively started Taylor flow (Takeda, Kobashi & Fisher 1990) and Görtler flow (Ikeda & Maxworthy 1990), in inclined free-convection boundary layers (Chen *et al.* 1991), and both merging and splitting of spanwise structures have been observed in acoustically forced shear layers (Browand & Prost-Domasky 1990). Natural convection of binary fluid mixtures constitutes another environment in which defects (merging and splitting) are observed (Bensimon *et al.* 1990).

Recent theories of phase-turbulence (Coullet & Lega 1988; Coullet, Gil & Lega 1989) propose that defects may move around in orderly wave patterns generating 'topological turbulence'. These studies are based mostly on two-dimensional model systems (Ginzburg–Landau equations), but the recent experiments of thermal convection of a binary fluid by Bensimon *et al.* (1990) in a large-aspect-ratio annular container reveal that 'the evolution of the transient can be largely described in terms of the production of defects'. They found that these defects allow a region of flow with one wavenumber to evolve spatially to another wavenumber. Similarly, the plane rotating Poiseuille flow simulations (with two periodic directions and a long spanwise length) by Yang & Kim (1991) indicate that a complex vortex merging process occurs, the outcome of which, at the statistically steady state, is to reduce the number of vortex pairs from seven to three. Ligrani & Niver (1988) in their experiments on curved channel flow report also that the vortices may undergo a repeated sequence of merging and splitting in a range of $Re/Re_c$ around two.

At Reynolds number sufficiently larger than $Re_c$ another destabilizing phenomenon takes place. It is termed the *secondary instability* of the Dean flow and corresponds to short-wavelength travelling waves. Theoretical studies on these waves have been performed by Finlay *et al.* (1987, 1988) through linear stability analysis and Navier–Stokes simulations, and Bennett & Hall (1988) who performed an asymptotic analysis. Experiments have been carried out by Kelleher, Flentie & McKee (1980), Ligrani & Niver (1988) and Matsson & Alfredsson (1990, 1992). Experimental results provided some confirmation of the theory. In particular, it appear that these waves – sometimes referred to as *twists* – go unstable at first in the region of low streamwise velocity where the flow moves away from the outer wall (Matsson & Alfredsson 1992) because of a shear instability (Finlay *et al.* 1987, 1988).

The present work considers a channel for which recent experimental measurements are available (Matsson & Alfredsson 1990, 1992; Bottaro *et al.* 1991; Matsson *et al.* 1991). The curvature ratio $\gamma$, equal to the ratio of inner radius $r_i$ to outer radius $r_o$, is taken to be 0.974. Since it is fixed, we will not introduce the Dean number (which depends on $\gamma$) but we will consider only the Reynolds number, based on the bulk velocity $U$ in the channel and the channel height, $h$. The area of the cross-section is denoted $A$. The mean radius of curvature of the channel, $\frac{1}{2}(r_i + r_o)$, is equal to $38h$. In the present parameter space, the critical Reynolds number $Re_c$ for the onset of Dean vortices is 225, and the critical wavenumber $\beta_c = 2\pi h/L$ is 3.97, where $L$ is the spanwise

wavelength. From linear stability theory (Finlay *et al.* 1987) it is found that the critical conditions depend on $\gamma$. The larger $\gamma$ is the higher $Re_c$ is and the smaller $\beta_c$. For fixed $\gamma$, the linearly most unstable wavenumber increases with $Re$, and, for example, at $Re/Re_c = 2.43$ it is equal to 5.76.

A channel of aspect ratio equal to nine with a periodic spanwise direction is considered in most of the computations. This length is sufficient to allow the development of several vortex pairs, so that wavelengths are selected naturally and not imposed†. This is an important requirement if vortex interactions resulting from the Eckhaus instability are to be considered.

The purpose of the present work is to carry out the first three-dimensional incompressible Navier–Stokes spatially developing simulations for an array of longitudinal vortices, under conditions of steady and fluctuating inlet forcing. Comparisons with available experimental data are provided and some insight into the physics is gained, particularly in the developing region. Further, we set out to verify numerically some of the phenomena described by Guo & Finlay (1991) concerning the Eckhaus instability and elucidate the importance of vortex interaction processes in the dynamics of the flow.

## 2. The relative merits of spatial versus temporal simulations

The numerical approach taken in this work is defined as the *spatially developing* approach, in contrast to the more commonly used *temporally developing* technique. In this section we will try to point out strengths and weaknesses of both approaches with reference to the specific case of curved channel flow, and justify our choice for performing spatial simulations.

The temporal approach mimics the flow development by relating the nonlinear streamwise development of the motion to the temporal one, while the spatial approach tries to reproduce it by the adoption of suitable inlet–outlet boundary conditions. Up to the onset of the secondary instability a temporally developing simulation is usually carried out on a two-dimensional calculation domain. A channel cross-section is considered and all streamwise derivatives in the equations of motion are eliminated (parallel-flow approximation). When streamwise gradients become significant (when, for example, streamwise waves – denoting the secondary instability – occur) a three-dimensional channel with periodic streamwise conditions is used. The flow is driven by a forcing term $S$, which represent an average streamwise pressure gradient. In channel flow, when $S$ is small the parallel-flow solution is a shifted parabola with the maximum towards the inner wall. This is the subcritical one-dimensional curved channel flow solution, sometimes referred to as CCPF (curved channel Poiseuille flow), and expressed as

$$u = U(1-\gamma)[c_1 \rho \ln \rho + c_2(\rho - \rho^{-1})],$$

with $$\rho = \frac{r}{r_0}, \quad c_1 = \left[\frac{\gamma^2}{1-\gamma^2}(\ln\gamma)^2 - 0.25(1-\gamma^2)\right]^{-1}, \quad c_2 = c_1\left(\frac{\gamma^2}{1-\gamma^2}\ln\gamma\right).$$

When $S$ increases above a critical value a steady vortical flow develops. By further increasing $S$ merging and splitting of vortex pairs take place. Such events can be unsteady in a temporally developing simulation, and repetitive merging and splitting events occur. If $S$ is held constant, oscillations in mass flow rate will result; if the mass

† Note, however, that the average wavenumber is bound to be a multiple of $2\pi/9$ (i.e. 4.19, 4.89, 5.59...).

flow rate is held constant, oscillations in average pressure gradient will result. The latter is the case of Guo & Finlay (1991), cf. their figure 20. At yet larger $S$, a secondary instability will set in. This is another source of unsteadiness. To mimic the spatial development one normally introduces a convection velocity in the streamwise direction and matches the experimental results (if they are available) *a posteriori*. Most of the features of the flow can then be reproduced. However, it should be noted that this convection velocity is, in general, not constant throughout the different flow regimes (see, e.g. Liu & Domaradzki 1990, for comments related to the Görtler problem); furthermore, there are no reasons why it should remain uniformly constant within the same cross-section at any given time or for the whole flow. One can envisage the occurrence of this situation at the onset of the secondary instability, when the upwash region of the vortices (where the flow moves away from the outer wall) starts oscillating on a fast timescale, whereas the rest of the flow remains stationary (Matsson & Alfredsson 1992). Typically, the agreement between experiments and computations based on the temporal model deteriorates as time increases; eventually, temporal simulations break down (see e.g. Liu & Domaradzki 1990). It is also noteworthy to mention that different simulations of the flow corresponding to the experiments of Swearingen & Blackwelder (1987) lead to the adoption of convection velocities differing from one another by 14% to achieve a proper matching (cf. Liu & Domaradzki 1990; Sabry & Liu 1991).

Another strong argument against temporally developing simulations invokes the *convective* nature of the instability. Although no decisive proof has yet been provided, it is generally accepted that Dean flow (as well as Görtler flow) represents a convectively, rather than an absolutely, unstable flow. Roughly speaking this means that imposed perturbations will grow and travel downstream. The importance of the distinction between convective and absolute instability has been highlighted by Huerre & Monkewitz (1990). When adopting streamwise-periodic boundary conditions in an incompressible flow, a disturbance anywhere in the flow would propagate upstream through the periodic boundary and the convective nature of the instability would be lost.

Finally, when analysing the secondary instability through temporally developing simulations, the streamwise wavelength will be dependent on the streamwise length of the computational domain. This is so because, due to streamwise periodicity, only an integer number of cycles (waves) can be accommodated within a fixed length. If the resulting wavelength is not the most unstable one (which is the wavelength likely to be selected naturally in an experiment) the predictions of frequency, wavenumber, type of instability (sinuous or varicose) etc., will be poor or, at the least, uncertain.

On the other hand, the spatial approach is not exempt from drawbacks, but they seem to be more easily dealt with. The main problem lies in the correct specification of open boundary conditions. If the physical flow conditions at the boundaries could be specified exactly there should be no error arising from the truncation of the domain. In practice, even this idealization does not hold, because the solution of the discretized equations does not match exactly the continuum field. As such, the specification of Dirichlet or Neumann conditions – which are, mathematically speaking, perfectly reflecting conditions – generates at the boundaries small perturbations which might be reflected back and forth in the computational domain. Since in the present flow situation a Dirichlet condition is used at the inlet, a non-reflecting outlet boundary condition should be used at the exit cross-section. A perfectly non-reflecting condition does not exist for incompressible flows, but it is possible to specify conditions that produce minimum numerical reflection back into the computational domain.

A more intricate phenomenon that is known to appear sometimes is a resonance effect between inlet and outlet sections. This is caused by the reflection of pressure waves between inlet and outlet boundaries (see Buell & Huerre 1988 and Huerre & Monkewitz 1990 for a discussion of the problem). The results is that a locally convectively unstable flow can be transformed into an absolutely unstable flow, with serious consequences for flow definition and control. The phenomenon is such that imposed (or naturally occurring) perturbations that are being convected outside of the domain are fed back, almost instantaneously, at the entrance of the domain itself. For the case of the Dean flow this undesirable effect (which is the analogue of the facility effect plaguing several experimental installations, Huerre & Monkewitz 1990) can be dealt with by the adoption of proper inflow conditions. By proper we mean Dirichlet conditions expressing the CCPF plus a steady perturbation of sufficiently large amplitude to overrule the fluctuating perturbation generated by the feedback mechanism. In §§4 and 5 results for the two cases of inlet flow steadily and randomly forced are presented.

## 3. Numerical technique

The governing equations of conservation of mass and momentum expressed in cylindrical polar coordinates $(\theta, r, z)$ are

$$\frac{1}{r}\frac{\partial u}{\partial \theta}+\frac{1}{r}\frac{\partial (rv)}{\partial r}+\frac{\partial w}{\partial z}=0,$$

$$\frac{\partial u}{\partial t}+\frac{1}{r}\frac{\partial (u^2)}{\partial \theta}+\frac{1}{r}\frac{\partial (ruv)}{\partial r}+\frac{\partial (uw)}{\partial z}=-\frac{1}{r}\frac{\partial p}{\partial \theta}+\frac{1}{Re}\left(\nabla^2 u+\frac{2}{r^2}\frac{\partial v}{\partial \theta}-\frac{u}{r^2}\right)-\frac{uv}{r},$$

$$\frac{\partial v}{\partial t}+\frac{1}{r}\frac{\partial (vu)}{\partial \theta}+\frac{1}{r}\frac{\partial (rv^2)}{\partial r}+\frac{\partial (vw)}{\partial z}=-\frac{\partial p}{\partial r}+\frac{1}{Re}\left(\nabla^2 v-\frac{2}{r^2}\frac{\partial u}{\partial \theta}-\frac{v}{r^2}\right)+\frac{u^2}{r},$$

$$\frac{\partial w}{\partial t}+\frac{1}{r}\frac{\partial (wu)}{\partial \theta}+\frac{1}{r}\frac{\partial (rwv)}{\partial r}+\frac{\partial (w^2)}{\partial z}=-\frac{\partial p}{\partial z}+\frac{1}{Re}\nabla^2 w,$$

where

$$\nabla^2=\frac{1}{r^2}\frac{\partial^2}{\partial \theta^2}+\frac{1}{r}\frac{\partial}{\partial r}\left(r\frac{\partial}{\partial r}\right)+\frac{\partial^2}{\partial z^2}.$$

The streamwise velocity is denoted $u$, the normal velocity is $v$ and the spanwise velocity is $w$. The scalings used are the channel height $h$ for length, the bulk speed $U$ for velocity, $h/U$ for time, and $\rho U^2$ for dynamic pressure, where $\rho$ is the (constant) density of the fluid. No-slip Dirichlet conditions for the velocity are applied at the solid boundaries. The spanwise direction is taken periodic. Open boundary conditions (inflow and outflow) need to be specified. In the present flow situation the outflow conditions constitute less of a problem than the inflow conditions. The reason for this is that for our problem there is no backflow at the outlet boundary and the flow there is almost parallel. As such, convective conditions such as the ones described by Lowery & Reynolds (1986) and Bottaro (1990) are suitable. Alternative open conditions proposed in the literature require the addition of buffer regions at the two ends of the physical domain. Danabasoglu, Biringen & Street (1989) use the buffer domain technique to solve for Tollmien–Schlichting waves in a two-dimensional computational domain. In their implementation the buffer domain has the same length and the same

number of mesh points as the physical domain. In three dimensions such a procedure is extremely demanding on computational resources.

For the reasons outlined above, we choose conditions expressing the vanishing of the average convective derivative of each velocity component. These conditions are suited to time-dependent problems and have been shown to produce negligible upstream reflection of outgoing waves in a Poiseuille/Bénard travelling wave problem (Bottaro 1990). In dimensionless units they read:

$$\frac{\partial u}{\partial t}+\frac{c}{r}\frac{\partial u}{\partial \theta}=0, \quad \frac{\partial v}{\partial t}+\frac{c}{r}\frac{\partial v}{\partial \theta}=0, \quad \frac{\partial w}{\partial t}+\frac{c}{r}\frac{\partial w}{\partial \theta}=0.$$

The quantity $c$ is a wave speed and in the present situation it has been chosen constant and equal to the bulk velocity. It was found that different choices of the phase velocity affect the solution only marginally in a limited neighbourhood of the exit cross-section. Similar behaviour has been observed by others (see e.g. Pauley, Moin & Reynolds 1990). The above conditions have been discretized in space and time by first-order schemes, as in Bottaro (1990). The inlet condition is CCPF with, eventually, a steady perturbation superimposed on to it to drive the vortex development and lock the vortices into place. The problem of inflow and outflow boundaries is crucial as discussed in §2, and possible consequences of the inlet–outlet conditions are addressed in §5. The angle subtended by the channel is taken to be equal to 100° in the steady forced case (§4) and 180° in the randomly forced case (§5). In both cases, the streamwise grid employs 130 points; this is sufficient to resolve the long streamwise scales of the motion before the onset of twists. The comparison with the linear theory for spatial growth of longitudinal vortices in $\theta$ (reported in §4) is particularly reassuring with respect to the streamwise numerical resolution, at least for small $\theta$. A fine resolution is employed in the cross-section and the grid, which is staggered, is composed of 160 uniformly spaced spanwise points and 24 normal points, smoothly stretched to resolve the boundary layers near the walls. Detailed comparisons with velocity profile measurements on different streamwise cross-sections provide partial confirmation that the mesh is adequate.

The spatial discretization, in the finite volume approximation, adopts a second-order central difference scheme to treat total (convective and diffusive) fluxes. Solutions are obtained by fully implicit time-marching. Inner iterations are performed at each time step to ensure that the maximum pressure and velocity residuals decrease by at least four orders of magnitude. The dimensionless time step $\mathrm{d}t$ is taken equal to 0.1. It is sufficiently small to provide confidence in the time accuracy of the numerical procedure: ten time steps advance a fluid element about one streamwise mesh width at speed $U$ on the longer channel. Smaller steps produce identical signals, while with bigger time steps ($\mathrm{d}t = 0.3$) slight deviations in time histories occur when there are sharp temporal gradients. The adoption of very small time steps is imposed, when the investigation of the real transient is the primary objective, because the time error is formally of first order. When we are only focusing on the steady-state solution the restriction on $\mathrm{d}t$ can be somewhat relaxed, although Yee & Sweby (1992) have elucidated some of the consequences of selecting 'large' time steps. (For example, the basin of attraction of a steady solution can be completely altered and spurious chaotic solutions may appear when the Courant number is chosen too close to one.) The SIMPLER pressure correction technique of Patankar (1980) is used to treat the pressure coupling. The computational domain is scanned with radial and azimuthal zebra relaxation sweeps. Three sweeps are performed for pressure and pressure correction equations and one each for the three momentum equations. This type of relaxation

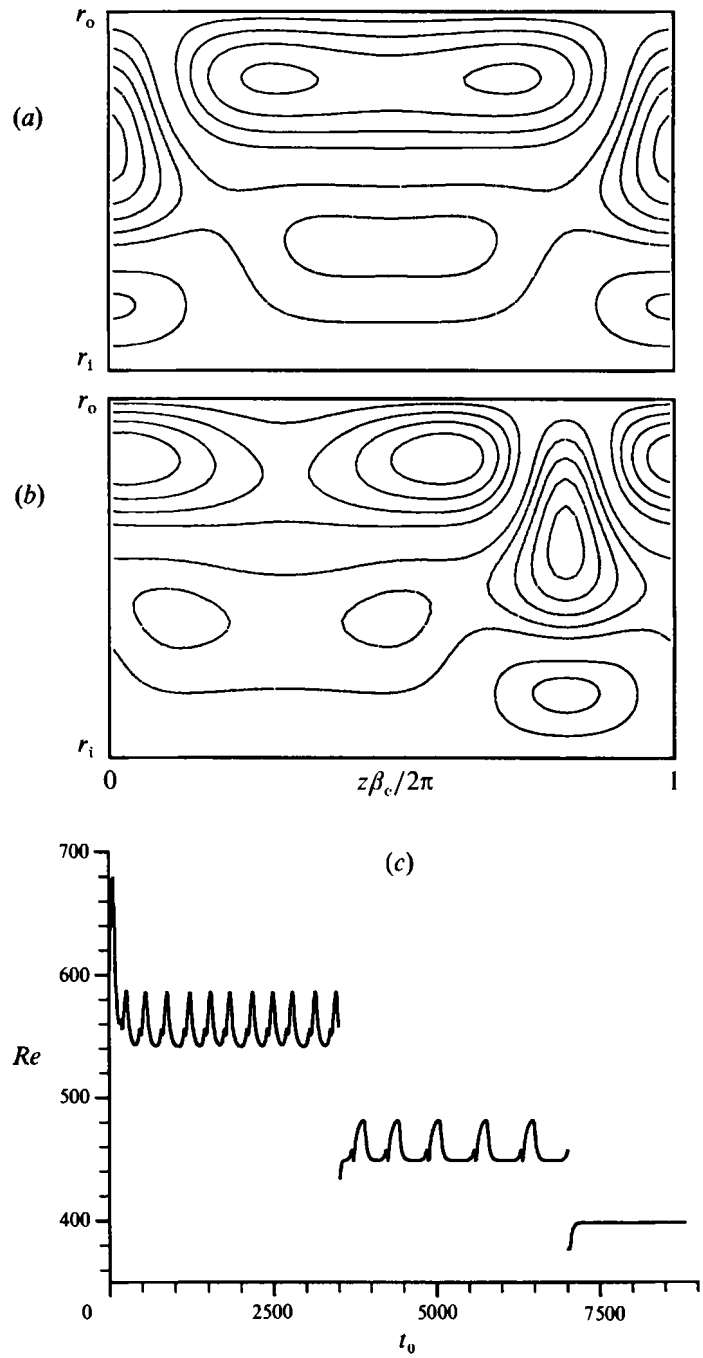


FIGURE 1. Isolines of (*a*) the streamwise perturbation velocity in the cross-section for a stationary axisymmetric flow, $Re = 397$ and (*b*) a time-dependent flow with an incipient splitting process by the outer wall, $Re = 563$. Isoline spacing is 0.075. In (*c*) the Reynolds number is plotted with respect to $t_0$ for, from the left, $Re_0 = 710, 550, 450$. In the first two cases the oscillations of mass flow rate at constant pressure forcing produce actual Reynolds numbers that vary in the intervals [542, 586] and [449, 481], respectively. In the third case shown the flow is stationary and $Re = 397$.

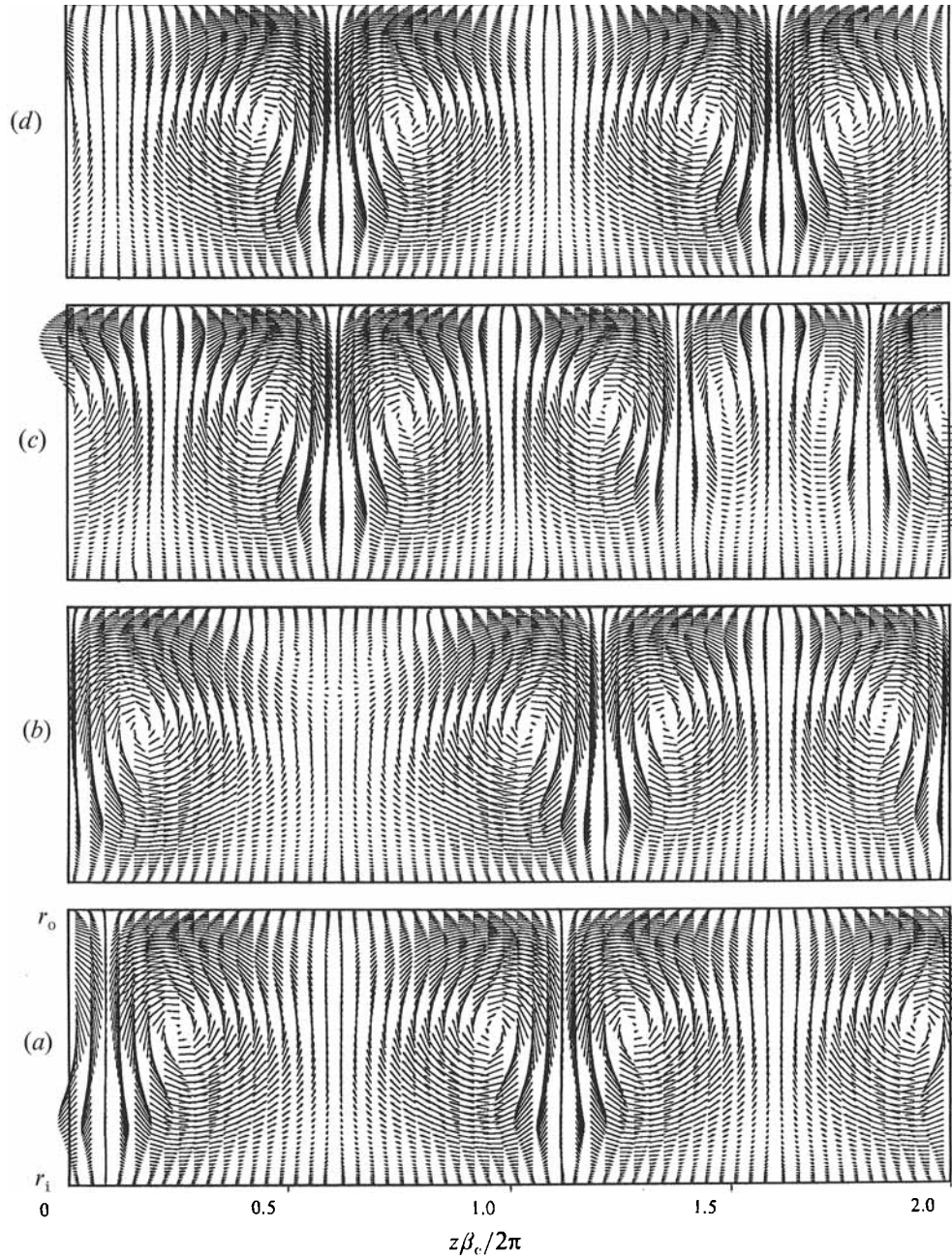


FIGURE 2. Secondary velocity field at time (*a*) $\tau$, (*b*) $\tau+125$, (*c*) $\tau+250$, (*d*) $\tau+375$, and with $Re =$ 397, 397, 384 and 393 respectively. Notice that by the end of the process the vortices have shifted by half a wavelength.

does not eliminate recursion but allows faster convergence than, for example, Gauss–Seidel sweeps, because all inner loops can be vectorized. The resulting tridiagonal systems of linear equations are solved by the use of the Thomas algorithm.

### 3.1. *Temporally developing results*

The code has been extensively tested against published results and against other codes. In particular, we report here on a comparison with the results of Finlay *et al.* (1987) for the case of axisymmetric curved channel flow. Two different computer codes have been employed for the comparison: the present one and one due to Marx (1991) which solves using finite volumes for the steady three-dimensional Navier–Stokes equations in general curvilinear coordinates, employing the artificial compressibility formulation. To compute axisymmetric results we have considered a three-dimensional domain of angular opening 10° and with streamwise periodic boundary conditions. The spanwise length of the domain is $2\pi/\beta_c$, with $\beta_c = 3.97$, and the curvature ratio $\gamma$ is 0.974. The initial condition is CCPF plus small random noise, $[-0.01, 0.01]$, on $u$. A constant forcing term $S$ is added to the $\theta$-momentum equation, equal to

$$S = \frac{1}{Re_0}\frac{2[32r^3 - 27r^2(r_i + r_o) + 5r_i r_o(r_i + r_o)]}{r^2(r_o - r_i)^2(r_i + r_o)}$$

and corresponding to the pressure gradient needed to drive CCPF at $Re_0$. $Re_0$ is the initial Reynolds number in the simulations when CCPF plus noise is used as initial condition. It is based on the bulk speed $U_0$. For supercritical conditions CCPF is unstable and the forcing is insufficient to maintain the initial mass flow rate; as a consequence the flow decelerates before reaching a final state, with Dean vortices, characterized by a new Reynolds number. This new Reynolds number is defined based on the computed average velocity. The steady results we obtain are converged to machine precision. Calculations have been performed on two grids, the finer of which contains $60^2$ points in the cross-section and 10 streamwise nodes. It should be noted, however, that the coarser mesh, employing $30^2$ nodes in the cross-section and 10 streamwise nodes, is enough to produce grid-converged results with both codes employed, in excellent agreement with the reference solutions. At $Re_0 = 500$ the artificial compressibility code fails to converge to a steady state, and the 'pressure correction' code shows a regular, time-periodic signal. The coarse-grid simulations overestimate the period of the oscillations of $Re$ by about 4%, and overestimate the amplitude of the oscillations by less than 1%, when compared to the fine-grid results. The signals of $Re$ in time are almost coincident, and the dynamics of the events found is the same with both grids.

In figure 1 the streamwise velocity perturbation (i.e. the near-parabolic undisturbed streamwise velocity profile has been subtracted) is shown for two values of the Reynolds number. Also plotted is the time behaviour of $Re$, for fixed constant forcing (fixed $Re_0$). (Note that time in figure 1 is $t_0$ and is made non-dimensional with reference to $U_0$, the velocity that defines $Re_0$.) The state with one vortex pair in the cross-section ceases to be stable for $Re/Re_c$ between 1.78 and 1.95 (Finlay *et al.* 1987, report $1.78 < Re/Re_c < 2.19$ while Bennett & Hall 1988, for a similar configuration, report results that suggest vortex doubling at $Re/Re_c \approx 2.3$). For $Re$ around 460 a periodic sequence of merging and splitting processes starts to take place. A similar situation was encountered in the numerical simulations of Dean flow by Ravi Sankar *et al.* (1988). A repetitive sequence of merging and splitting has also been observed experimentally by Ligrani & Niver (1988) for $Re/Re_c \approx 2$, $\gamma = 0.979$. The occurrence of this phenomenon

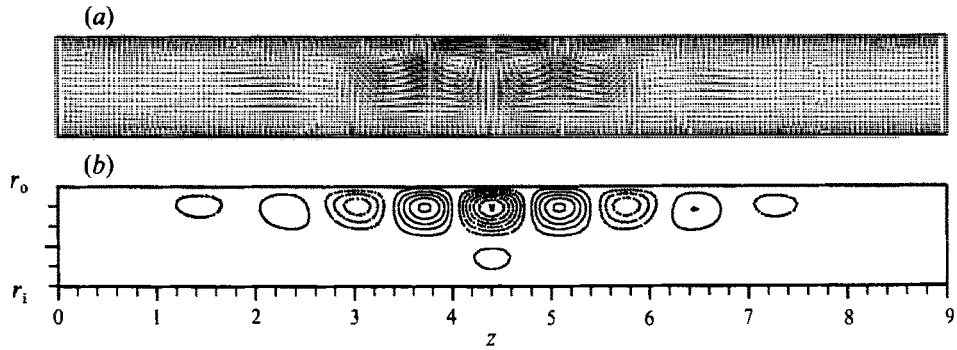


FIGURE 3. Initial velocity field for the simulations: (*a*) secondary flow; (*b*) deviation of $u$ from CCPF. Interval in the isolines of $u'$ is 0.003; zero lines omitted. Here $-0.021\,144 \leqslant u' \leqslant 0.015\,595$, $-0.001\,423 \leqslant v \leqslant 0.001\,243$, $-0.001\,336 \leqslant w \leqslant 0.001\,483$.

has been predicted by Guo & Finlay (1991) who found that when the wavenumber of the basic flow is equal to 3.97, the parallel-flow state is always unstable to spanwise perturbations for $Re/Re_c$ as low as 1.14 (cf. their figure 6). The latter explains the presence of oscillations in figure 1(*c*). The forcing $S$ supplied ($Re_0 = 450$) is sufficient to drive a flow characterized by one vortex pair in a box of spanwise length $2\pi/\beta_c$ at $Re = 397$. When the forcing is increased, the Reynolds number tends to grow and a splitting is attempted. The pressure gradient is however insufficient to maintain the two pairs of Dean vortices in the box chosen so that the splitting is reversed and $Re$ decreases. The same periodic behaviour is described by Guo & Finlay (1991, figure 19), whereas Finlay *et al.* (1987) find a steady solution with two vortex pairs for $Re$ as large as 492 in a box of spanwise wavenumber $\beta_c$. The latter finding could possibly be explained by a non-uniqueness of the axisymmetric solutions. The fact of not having found merging and splitting in the present simulations for $Re$ as large as 1.78 $Re_c$ is caused by having chosen a computation box of small spanwise wavelength.

When a channel of twice the spanwise length is considered the Eckhaus instability mechanism manifests itself earlier. This is shown in figure 2, where the secondary flow in the cross-section is plotted at four points equidistant in time, within one period. Here we have chosen $Re_0 = 450$, and it is found that $Re$ oscillates regularly between 384 and 397. At time $\tau$, $Re$ is at its maximum and two vortex pairs coexist in the cross-section. They are exact replicas of the vortex pair shown in figure 1 (*a*). At $\tau + 125$ (dimensionless time interval is in units of $t_0$) $Re$ is still at its largest but in the region for which $z\beta_c/2\pi \approx 0.6$ a splitting starts near the concave wall. As the splitting takes place (and the new vortex pair grows in strength) neighbouring pairs move apart forcing a merging at $z\beta_c/2\pi \approx 1.6$. This event, consisting of the annihilation of two neighbouring counter-rotating cells is completed at $\tau + 375$. At this time the vortices present at $\tau$ seem to have moved by half a wavelength in the spanwise direction. This apparent movement is a direct consequence of the merging and splitting events. Exactly the same sequence of events is described by Guo & Finlay (1991) in their figure 19, for a $Re$ held constant and equal to 400 (Guo & Finlay take the option of working at constant mass flow rate and variable average pressure gradient).

Before concluding this section we emphasize two points:

(i) The spanwise length of the computational domain is one of the factors that determines vortex interaction behaviour when the temporal model is employed;

(ii) We have found periodic merging and splitting events in a temporally developing

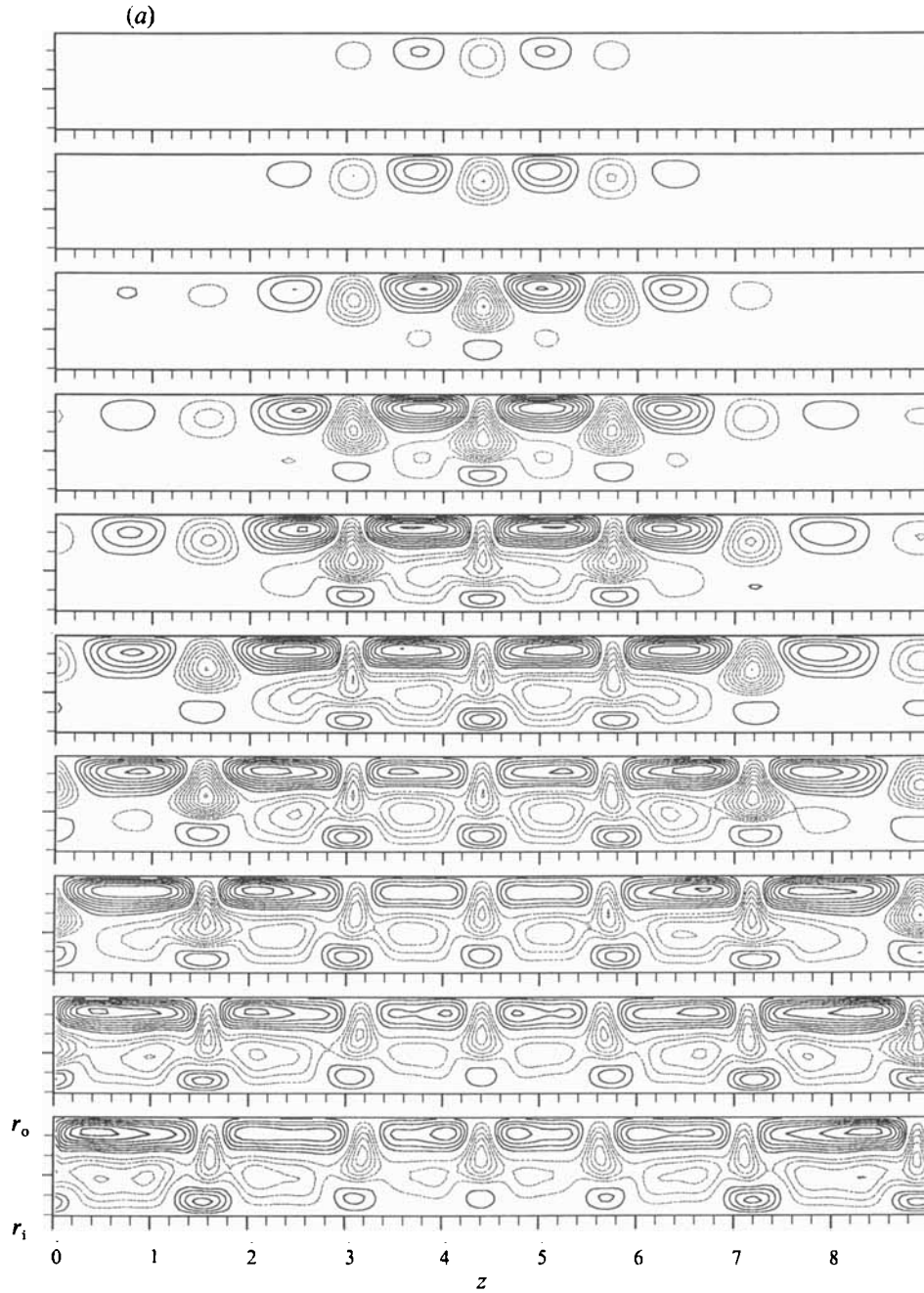


FIGURE 4(*a*). For caption see facing page.

simulation, in contradiction with the experiments of Matsson & Alfredsson (1992) which describe steady merging and splitting events.

In the remainder of the paper we abandon the temporal approach to pursue the spatially developing one.

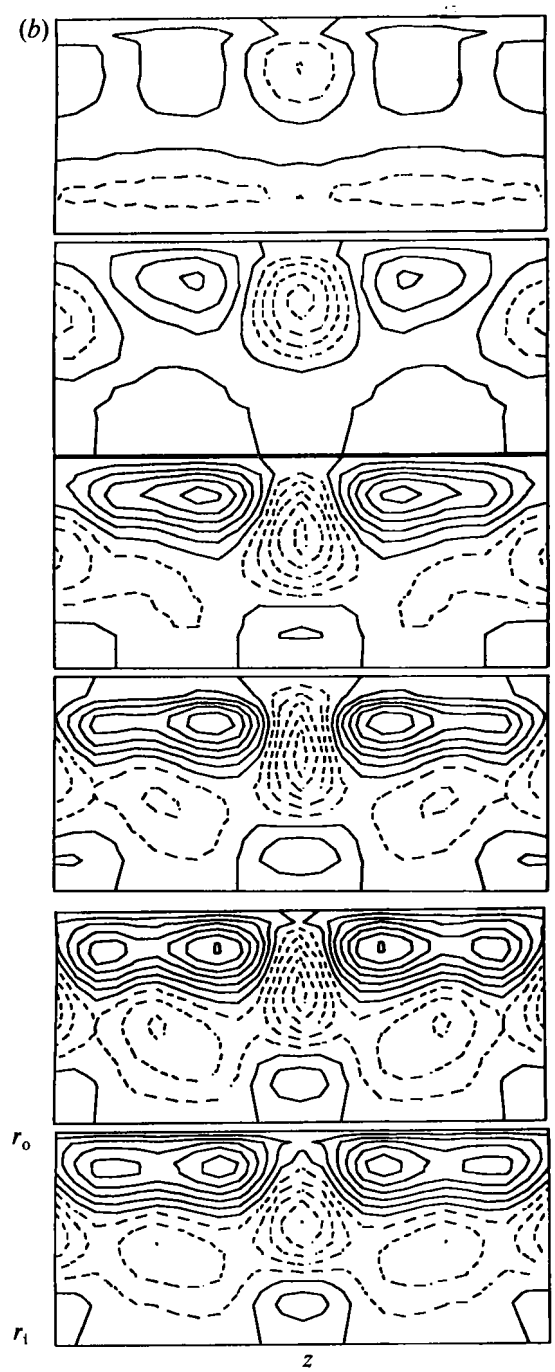


FIGURE 4. (*a*) Streamwise perturbation velocity at $Re = 547$. (*b*) Ensemble averages of the measurements of Matsson & Alfredsson (1992). Angular spacing between consecutive sections is 0.192.

## 4. Steady Dean flow; controlled inlet forcing

In what follows the developing flow for $Re > Re_c$ is studied through spatial simulations which employ the inlet–outlet boundary conditions discussed in §3. To trigger the vortex development, a steady inlet perturbation characterized by vortices in

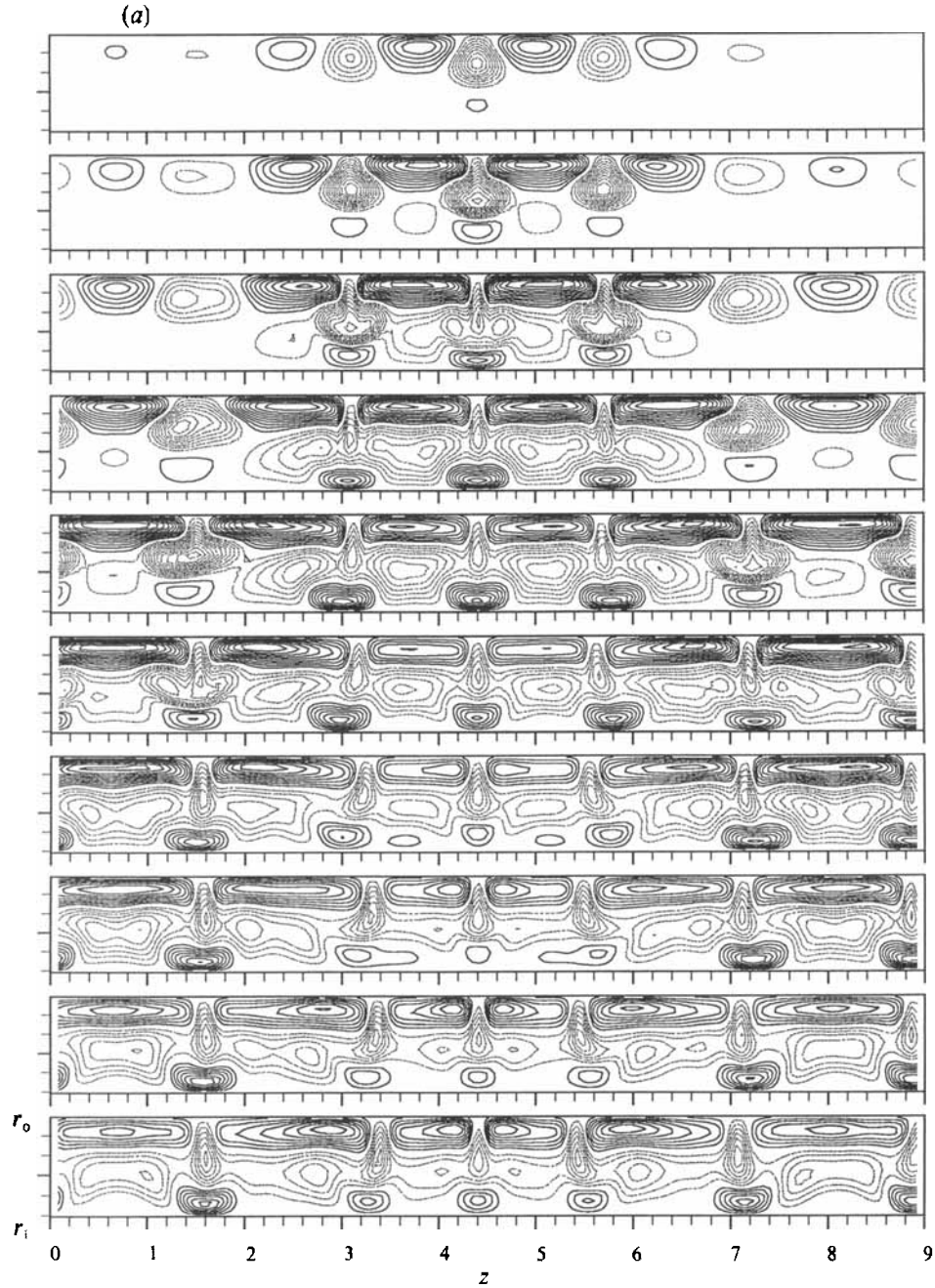


FIGURE 5(*a*). For caption see facing page.

their early linear stage is applied on top of the CCPF. The inlet solution could have been taken from the eigenfunctions of the linear analysis, but we have chosen instead to use a divergence-free velocity field taken from a previous simulation (see §5). This choice allows the presence of vortices at different development stages and with different individual wavelengths in the cross-section, a situation which is close to the experimental conditions. In figure 3 we show the flow field used as inlet (and initial) condition for the simulations described in this section. If we define the difference

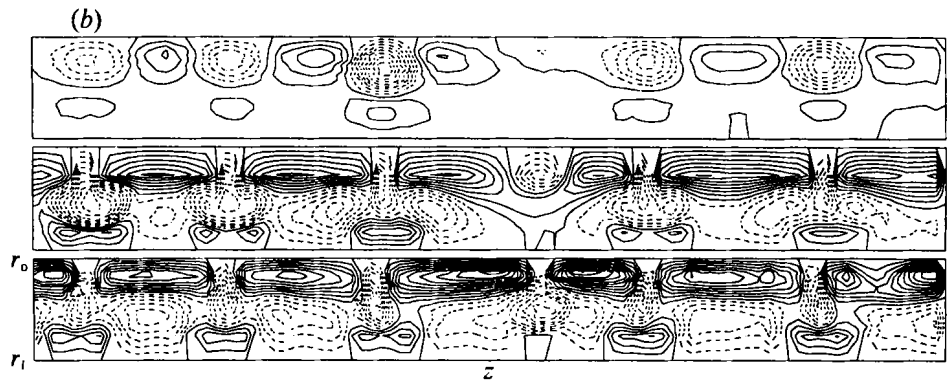


FIGURE 5. (*a*) Streamwise perturbation velocity at $Re = 970$. (*b*) Measurements of Matsson & Alfredsson (private communication). Angular spacing between consecutive sections is 0.384.

between the streamwise velocity and the CCPF as $u'$, the inlet condition chosen is characterized by

$$\bar{u} = \left(\frac{1}{A}\int_A u'^2 \,\mathrm{d}r\,\mathrm{d}z\right)^{\frac{1}{2}} = 0.0035741,$$

$$\bar{v} = \left(\frac{1}{A}\int_A v^2 \,\mathrm{d}r\,\mathrm{d}z\right)^{\frac{1}{2}} = 0.0003077,$$

$$\bar{w} = \left(\frac{1}{A}\int_A w^2 \,\mathrm{d}r\,\mathrm{d}z\right)^{\frac{1}{2}} = 0.0003887,$$

where $\bar{u}$, $\bar{v}$ and $\bar{w}$ represent average perturbation quantities and $A$ is the cross-sectional area of the channel. As a reference we should remember that the average streamwise velocity of the CCPF (which is used as velocity scale) is equal to one.

The flow fields obtained for $Re = 547$ ($Re/Re_c = 2.43$) and 970 (4.31) are stationary. They are shown, together with experimental results obtained on the same configuration by performing hot-wire measurements in air, in figures 4–7. The Reynolds numbers considered are, respectively, 14 and 8 times smaller than the critical Reynolds number for the growth of Tollmien–Schlichting waves in plane Poiseuille flow. Additionally, $Re = 970$ is smaller than the experimentally measured transitional $Re$ value for plane Poiseuille flow. In figures 4 and 5 we have plotted the streamwise disturbance velocity at different cross-sections. The sections shown in figures 4(*a*) and 5(*a*) correspond to, from the top, $\theta = 0.532$, 0.668, 0.804, 0.941, 1.077, 1.214, 1.350, 1.486, 1.623, 1.745. The angular spacing between two consecutive cross-sections is 0.136 (except for the last two cross-sections). The spacing of the isolines is 0.075, in all of the curves presented, unless otherwise indicated; negative perturbation velocities are shown dotted (or dashed), positive velocities are shown with continuous lines, the zero line is omitted. In figure 4(*b*) an ensemble average of the experimental measurements, with the mirror symmetry about the radial upwash plane explicitly enforced, is shown for $Re = 547$. The angular spacing between consecutive cross-sections is equal to 0.192. Pictures of the complete cross-sections measured have already been presented in Bottaro *et al.* (1991). For $Re = 970$ experimental results on three cross-sections spaced an angle of 0.384 apart from each other are shown in figure 5(*b*).

The first thing to remark is that the vortices in the simulations are locked into place without 'wandering' in the spanwise direction, in full agreement with the experiments with which we are comparing, and evolve steadily from the inlet to the outlet section.

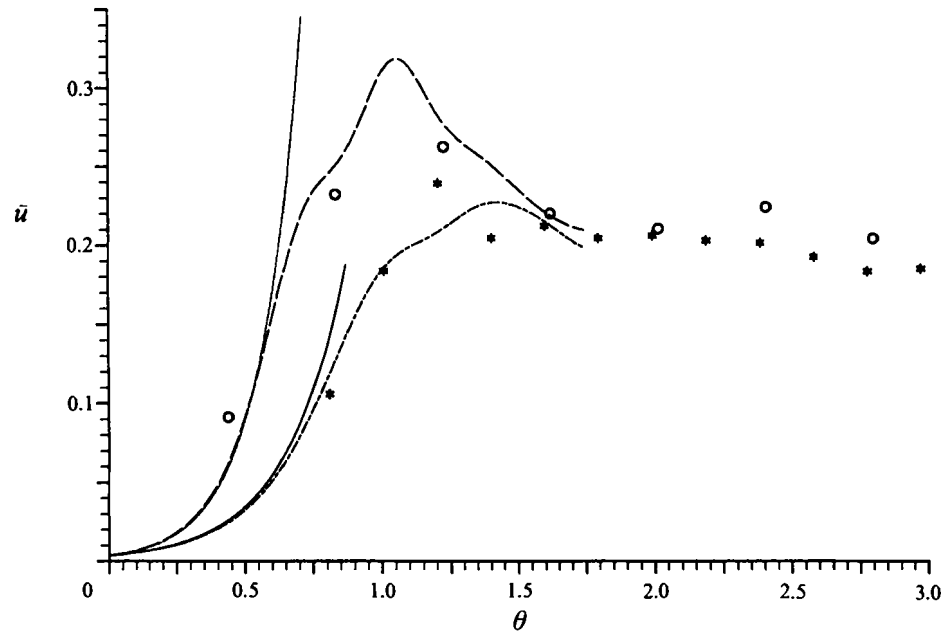


FIGURE 6. Computed average streamwise perturbation velocity $\bar{u}$ versus $\theta$, for $Re = 547$ (--------) and $Re = 970$ (------). Corresponding linear stability results are shown as continuous lines. Experimental results by Bottaro *et al.* (1991) at $Re = 547$ (*) and Matsson & Alfredsson (1992) at $Re = 970$ (○).

The absolute streamwise positions are not significant, since the inlet disturbance levels in experiments and simulations are different, so that a direct comparison would be meaningless. Rather, we compare the numerical results with the measured ones after shifting the experimental origin in $\theta$ so as to match its disturbance level with the disturbance level present in the simulations. One such comparison is presented in figure 6 where we have plotted $\bar{u}$ versus $\theta$. There we have also plotted the curves of linear spatial growth for the two Reynolds numbers considered and for $\beta = 4.89$ (which is the average wavenumber in the simulations).† They are represented by the function

$$0.003\,574\,1 \exp[m\theta/\eta],$$

where $\eta = 2(r_o - r_i)/(r_o + r_i)$, $m = 0.1202$ at $Re = 547$ and $m = 0.1698$ at $Re = 970$. The agreement between linear theory and the Navier–Stokes results is excellent up to $\theta = 0.6$. At this $\theta$, a very large disturbance amplitude in $u$ (of the order of 10% of the bulk velocity) is reached and nonlinear effects become important. Notice in figures 4(*a*) and 5(*a*) that regions of positive and negative perturbation at $\theta = 0.532$ have an approximately circular shape, as one would expect in the linear disturbance range, and are concentrated near the concave wall. Negative perturbations are associated with low-momentum fluid moving away from the outer wall, while positive perturbations are accompanied by movement of high-velocity fluid towards the wall. Further downstream, the positive perturbation regions tend to elongate in $z$ (near the concave surface) and squeeze, locally, the negative perturbations. The negative perturbations

† The most unstable wavenumber from linear stability at $Re = 2.43Re_c$ is equal to 5.76. According to Guo & Finlay (1991) the wavenumber here should, however, be selected by the Eckhaus instability, and be approximately equal to 4.6. The experiments by Bottaro *et al.* (1991) show an initial average wavenumber equal to 5.8, which decreases downstream, because of merging processes, to 4.5. Large individual variations in $\beta$ are present.

achieve a pear-shaped form (see typically the central vortex pair for $\theta = 0.941$, $Re = 547$ and $\theta = 0.668$, $Re = 970$). This shape is associated with a peak in $\bar{u}$. The maximum perturbation values here reach 60% and 80% of the bulk velocity for the two Reynolds numbers considered, respectively, in both experiments and simulations.

At larger streamwise distances what we may define as a quasi-parallel velocity profile (not strictly parallel according to the definition, but with slowly evolving structures) is attained by most of the vortex pairs (see, in particular, the central vortex pairs in figures 4*a* and 5*a*), and is reached more rapidly at larger Reynolds numbers, in agreement with the experiments. The average amplitude of streamwise perturbation for $Re = 547$ saturates (figure 6) to the value of 0.2 in the experiments. In the quasi-parallel state, while regions of fluid of negative perturbation velocity in a cross-section are similar to each other, elongated regions of positive velocity near the outer wall have different intensity of perturbation and spanwise length. Individual wavelengths in the cross-section differ by up to 100% for the larger Reynolds number simulated.

Events such as steady merging and/or splitting of vortex pairs are not observed because the test section is too short; however, Matsson & Alfredsson (1992) have shown experimentally that this is the case. The experimentally determined r.m.s. values of the streamwise perturbation velocity at different $\theta$ differ slightly from the computed results. The reason has to be found in the fact that vortices at different stages of development (and therefore with different amplitudes of perturbation) coexist in each cross-section in both experiments and simulations. In the numerical simulations, where the complete spatial development is available, the fact of having vortices at different stages of growth is evidenced, for example, by the presence of inflexion points in the $(\bar{u}, \theta)$-planes of figure 6, close to $\theta = 1.10$ for $Re = 547$ and $\theta = 0.75$ for $Re = 970$. This is clarified in figure 7, where the streamwise disturbance velocity is plotted in a $(z, R\theta)$-plane, where the radius $R$ is chosen equal to 38.457, that is 0.1382 units of length away from the concave wall. One sees that the central vortex pair experiences a maximum in positive perturbation amplitude at $R\theta \approx 40$ ($\theta = 1.04$) at $Re = 547$ and $R\theta \approx 30$ ($\theta = 0.78$) at $Re = 970$. Lateral pairs have a maximum in perturbation amplitude farther downstream. This development is consequent to the inlet condition, whereby the central vortex pairs at the entrance of the channel have a larger amplitude than the pairs near the periodic surface ($z = 0, 9$). The results obtained at these two Reynolds numbers are steady. At such $Re/Re_c$ ratios (respectively, 2.43 and 4.31) a secondary instability in the form of streamwise travelling waves (Kelleher *et al.* 1980; Finlay *et al.* 1987, 1988; Matsson *et al.* 1991, Matsson & Alfredsson 1992) is reported to occur. A secondary instability would have taken place if a proper time-dependent perturbation had been applied at the channel inlet to trigger the streamwise wave. This point will be discussed further in §6.

Some of the computed vortices show a loss of symmetry about the vertical upwash plane. This is more apparent at the larger Reynolds number and in vortices that are in a quasi-parallel state but not at their most 'energetic' state (i.e. the perturbation kinetic energy of the vortex pair is not at a maximum level). This bending of the vortices comes from attraction or repulsion of neighbouring vortex pairs caused by the Eckhaus instability, which is operational at the Reynolds numbers considered (cf. also the experimental results showing vortex interactions in Matsson & Alfredsson 1992).

The streamwise positions $\theta$ of largest amplitude of perturbation $\bar{u}$ correspond to those of largest spanwise-averaged (concave) wall shear stress, for both the Reynolds numbers examined. Figure 8 shows the development of wall shear stress $|\partial u/\partial r|_w$ for $Re = 547$ and 970, on the concave and convex walls. The values plotted are averages over the central vortex pair only, for $3.8 \leqslant z \leqslant 5$. Also, the wall shear at $z = 4.4$,

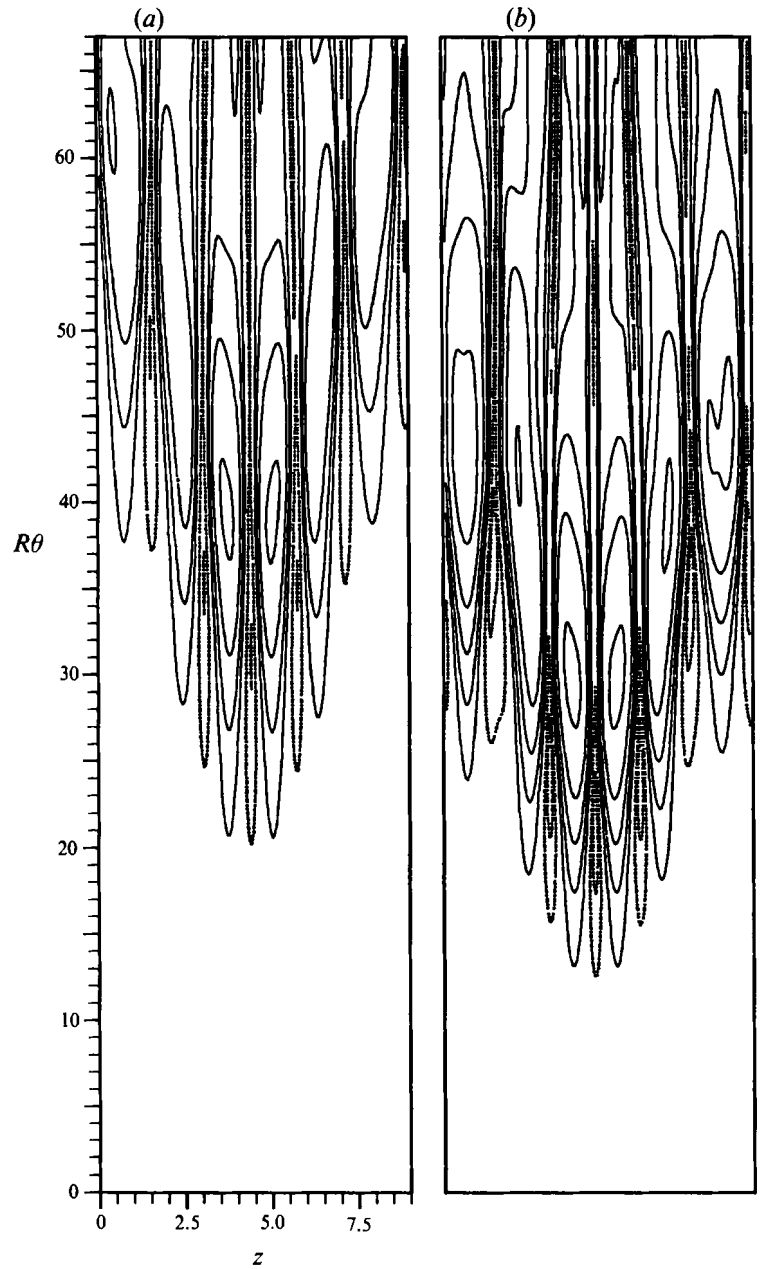


FIGURE 7. Streamwise perturbation velocity in an $(R\theta, z)$-plane at $R = 38.457$ for (*a*) $Re = 547$ and (*b*) $Re = 970$. Isoline spacing is 0.15 and the zero line is omitted. The horizontal scale is stretched by a factor of two as compared to the vertical scale.

corresponding to the upwash plane of the central vortex pair, is shown. At small streamwise distances the average values computed over inner and outer walls correspond exactly to those of CCPF, that is, respectively, 6.053 and 5.948. The dimensionless wall shear for plane Poiseuille flow is 6. Deviation in wall shear from the value corresponding to CCPF starts first on the outer wall, which is the wall unstable according to Rayleigh circulation criterion (see also Floryan 1991). Tiny Görtler-like vortices, developing at first near the outer wall grow downstream; as they grow they

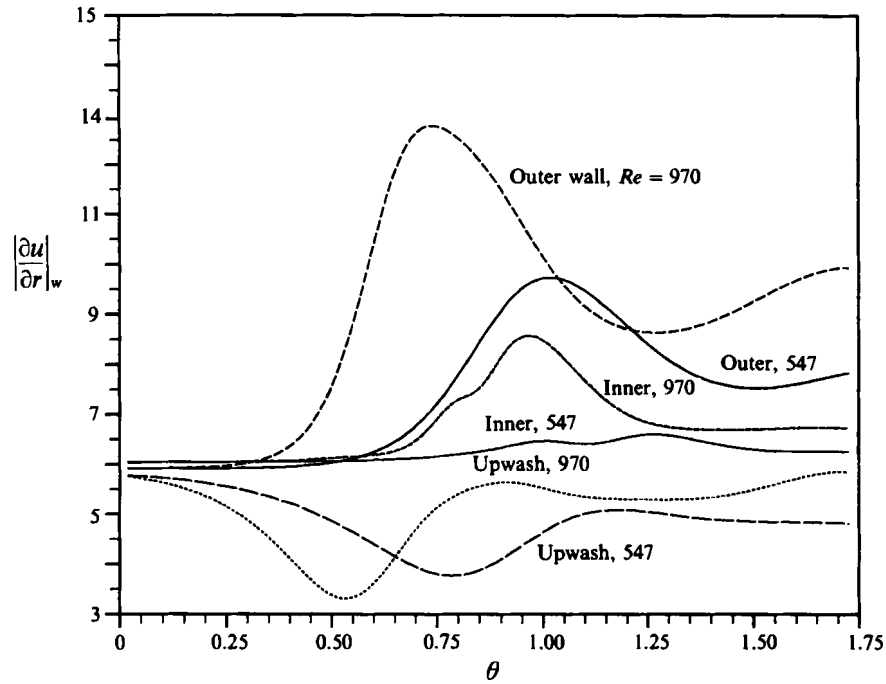


FIGURE 8. Streamwise development of wall shear stress.

affect the velocity distribution near the inner wall and modify accordingly the wall shear stress there. The average value of the wall stress increases up to a maximum on both curved walls; the maximum value depends on $Re$, and it is more than twice as large as the CCPF value at $r = r_0$, $\theta = 0.73$, $Re = 970$. This maximum corresponds closely to a maximum in positive streamwise perturbation velocity (cf. figure 7). Further downstream, the inner wall experiences a maximum in wall shear. Average values of wall shear on the curved walls decrease then to relative minima; the outer wall experiences a subsequent slow increase till the exit of the channel, while the inner wall reaches a quasi-constant value which is, for both $Re$ shown, slightly larger than the one corresponding to plane Poiseuille flow. In the upwash plane, where the streamwise velocity of the fluid is low, the wall shear decreases rapidly to a minimum at $\theta = 0.53$ (0.78) for $Re = 970$ (547). These points correspond to where the streamwise velocity reaches minimum values at $z = 4.4$ (cf. figure 7). Further downstream the wall shear in the low-speed region tends to rise and go towards an equilibrium value. The trends described apply to both Reynolds numbers examined; the development is faster for the large Reynolds number. It is noteworthy that the behaviour encountered closely resembles that described by Swearingen & Blackwelder (1987) for Görtler vortical flow for streamwise distances prior to the beginning of the secondary instability (cf. their figure 10).

## 5. Continuously self-forced flow

When only CCPF is imposed as a boundary condition at the inlet of the channel the situation encountered by Lowery & Reynolds (1986), Buell & Huerre (1988) and Huerre & Monkewitz (1990) may arise. It consists of a natural self-excited state that might be triggered, in a computational domain of finite streamwise extent, in the absence of external forcing at the inflow section. A persistent fluctuating field in the

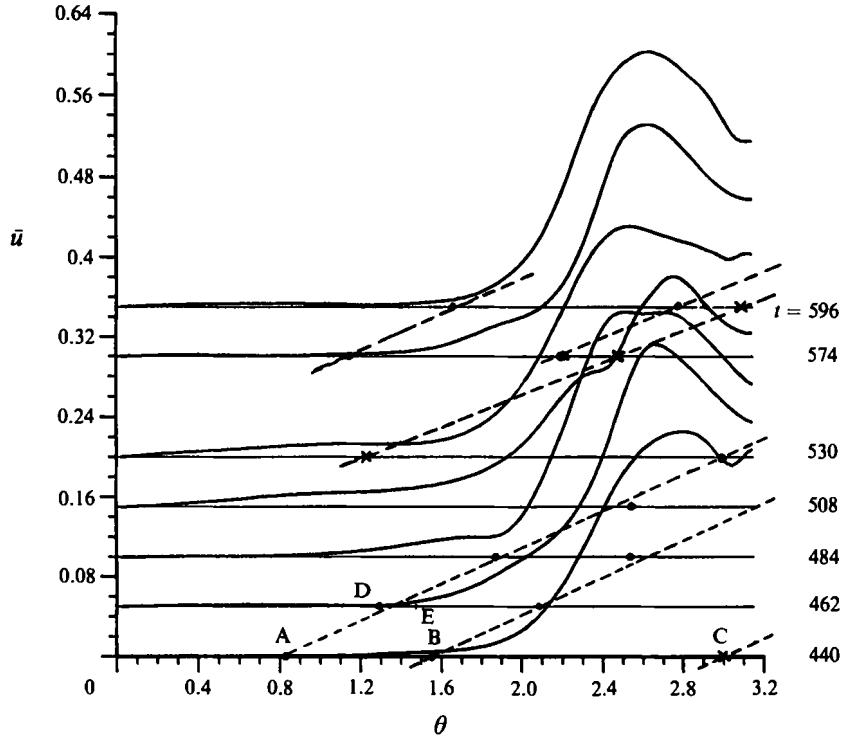


FIGURE 9. Average velocity perturbation $\bar{u}$ versus $\theta$ in the continuously forced case at seven different instants in time. Splitting is represented by ● and merging by ×.

convectively unstable Dean flow could normally be maintained only by an external forcing. In the present case the self-excitation is generated by a global resonance in the domain. Buell & Huerre (1988) state that 'the interaction between the vortical structures and the downstream boundary generates global irrotational pressure disturbances which are immediately transmitted to the inflow boundary. These are in turn converted into hydrodynamic instability waves by the inflow boundary condition'. This mechanism is equivalent to continuously and unsteadily forcing the inlet flow.

As shown by Guo & Finlay (1991), when perturbations are present the parallel Dean flow is always unstable to an Eckhaus instability for $Re > 1.2Re_c$ and $\gamma = 0.975$. Here we treat the case $Re = 2.43Re_c = 547$; as initial condition we apply CCPF throughout the computational domain, and allow round-off errors to act as infinitesimal perturbations to trigger the Dean instability. In figure 9, the variation of $\bar{u}$ with $\theta$ at different times is plotted. For $t > 440$ the curves are staggered in the vertical direction by an amount proportional to $(t-440)$. Defects (merging and splitting) are present. They appear as 'kinks' (inflexion points or relative extrema) in the plots of figure 9, and some of them are indicated by A, B, C and D in figures 9 and 10. For example, there are three defects at $t = 440$ (cf. figures 9 and 10*b*), and defect A moves to D at $t = 462$. Figure 10(*b*) shows defects already appearing near the inlet and propagating downstream at a speed approximately constant and equal to the bulk velocity of the flow. The movement of the defects is represented by the dashed lines in figure 9. The quantity $\bar{u}$ is always equal to zero by definition at $\theta = 0$, but it may grow immediately past the entrance because of the acceleration caused by the pressure perturbations. The maximum amplitude of the fluctuating perturbation, which is continuously generated a little downstream of the inlet of the channel (i.e. before the beginning of the linear

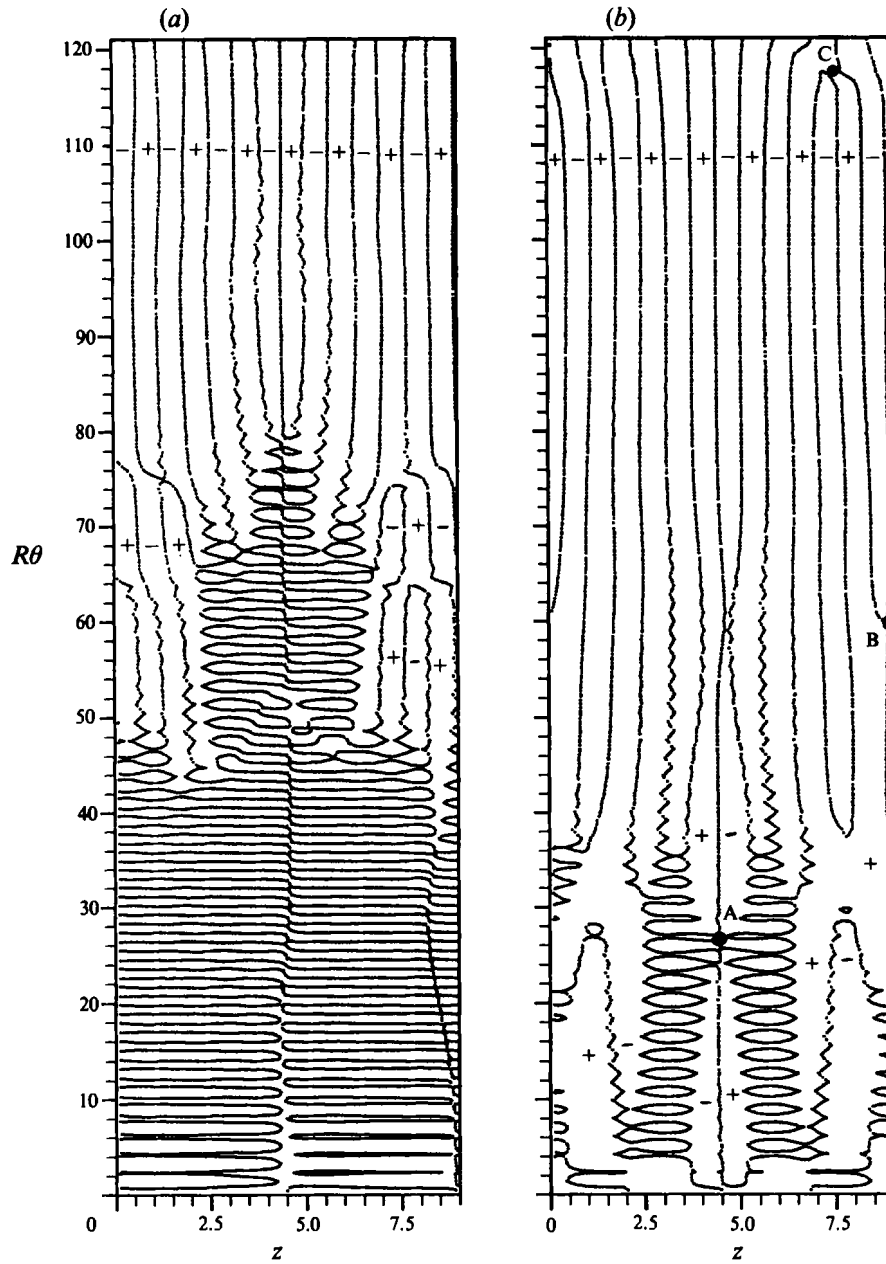


FIGURE 10. Isolines of zero spanwise velocity in an $(R\theta, z)$-plane; (*a*) $t = 358$ and (*b*) $t = 440$. Horizontal scale stretched by a factor of four.

amplification) varies in time, as shown in figure 9; however the adoption of a sufficiently large steady perturbation superimposed on to the CCPF profile is capable of stabilizing the flow.

For the simulations in §4, the chosen input flow field corresponds to the flow at the instant $t = 462$ and at $\theta = 1.45$ (shown with an E in figure 9). In the absence of such a steady forcing, defects propagating downstream may reappear near the inlet at later times. This is exemplified in figure 10 where regions of negative (−) and positive (+) spanwise velocities are represented. In this figure the zero-spanwise-velocity isolines are

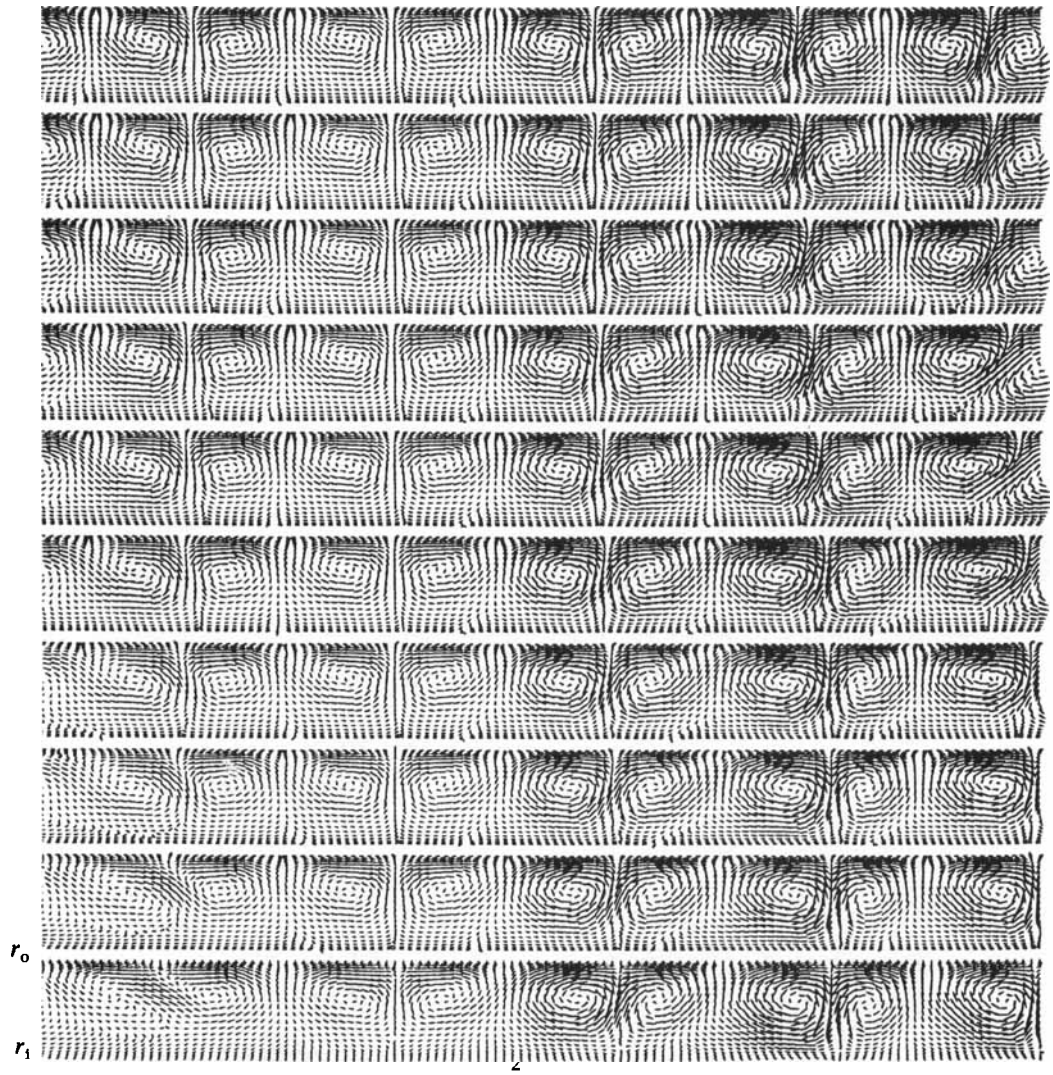


FIGURE 11. A two-to-one merging process involving vortex pairs across the periodic boundary. Angular spacing between consecutive cross-sections is 0.025. Upstream section at the top.

plotted and only random noise in $w$ is present at $t = 358$ at the entrance of the channel (figure 10$a$). Dean vortices grow out of the noise for $R\theta > 50$ near the periodic boundary. At $t = 440$ (figure 10$b$) near the inflow boundary there is an organized structure which corresponds to the vortical structure forming near $z = 4.5$ and $R\theta \approx 80$ at $t = 358$. Furthermore, all the vortices in the cross-section for $R\theta > 80$ have moved in $z$ by half a wavelength, so that the areas where $w$ is positive at $t = 358$ have negative $w$ at $t = 440$ and vice versa. This latter fact is due to the occurrence of defects. One such defect, a merging of vortex pairs, is noticeable, for example, in figure 10($b$) (point C) near the exit of the channel and it reduces the number of pairs across the span from seven (average wavenumber $\beta$ is equal to 4.89) to six ($\beta = 4.19$). Such defects represent an important phenomenon in the dynamics of longitudinal vortices. Both stationary (Matsson & Alfredsson 1990, 1992) and time-dependent (Ligrani & Niver 1988) merging and splitting processes have been reported in the Dean flow literature.

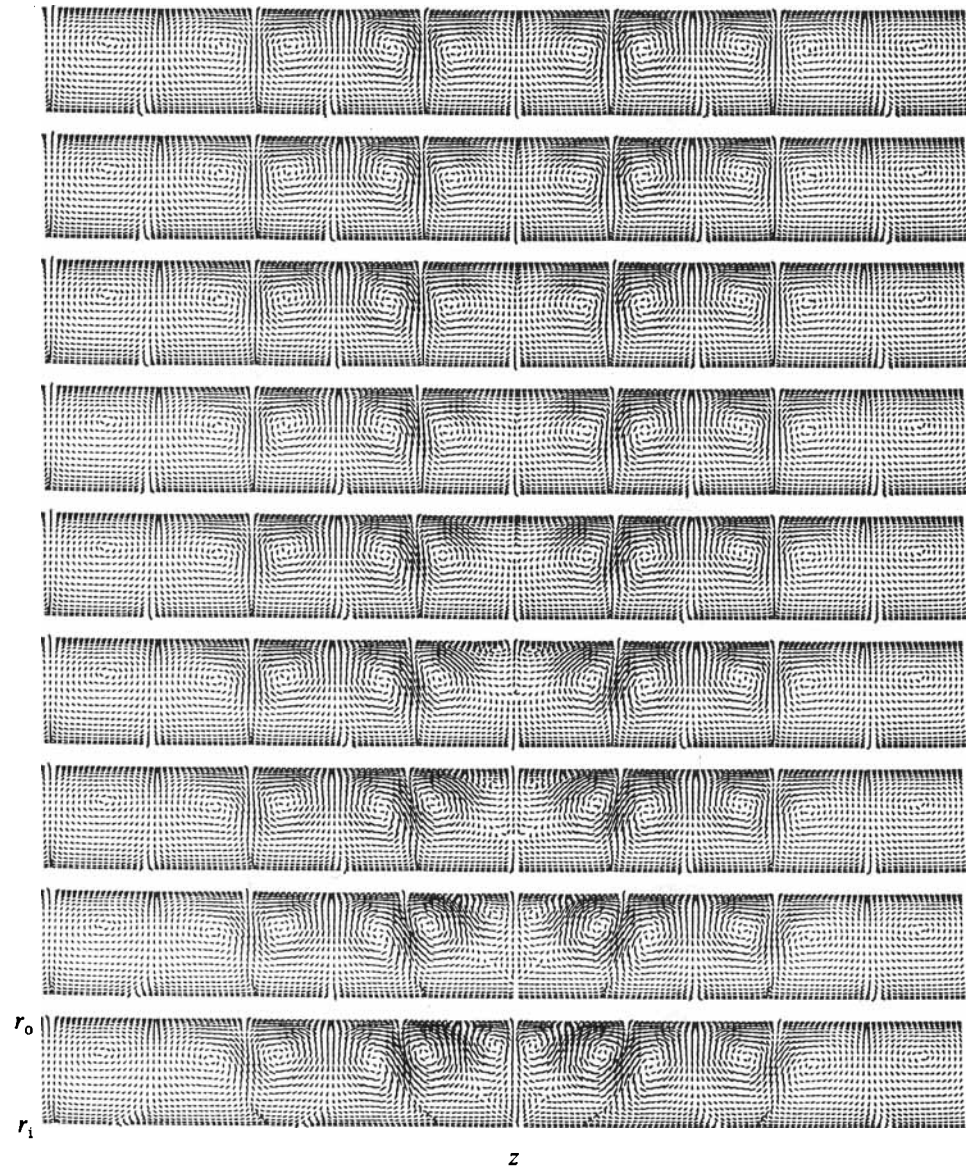


FIGURE 12. A two-to-three splitting process halfway through the span of the channel. Same streamwise spacing as in figure 11.

Similar events occur in the Görtler problem: Bippes (1978) describes the stationary appearance of new Görtler vortices that appear to 'pop' out of the concave wall in correspondence with the downwash plane of an existing pair, and on the steady merging of two neighbouring pairs into one new pair. Ito (communicated to Floryan 1991, p. 266) and Peerhossaini & Wesfreid (1988) describe Görtler vortices that are not locked into place and wander throughout the cross-section. We may thus distinguish between two situations. If the vortices are triggered by stationary disturbances they lock into place and grow downstream. Eventually, two vortex pairs may merge into one or a new pair may grow out of the concave wall. If low-amplitude or fluctuating disturbances are present in the approaching flow the vortices are not locked into place and may seem to wander across the span because of repetitive

merging and splitting processes (see also §5.1). In both cases the underlying driving mechanism for merging and splitting events is the wavelength selection mechanism, which is related to the Eckhaus stability of the vortices with respect to spanwise perturbations (Guo & Finlay 1991). Loosely speaking, if two vortex pairs are too close to each other they may merge into one pair, and if they are too far apart a new pair grows to fill the gap between the two original pairs.

Details of a merging event are presented in figure 11. There, for $t = 440$ and $Re = 547$, it is seen how two vortex pairs across the periodic boundary proceed to annihilate two neighbouring counter-rotating cells. This corresponds to event C in figure 9, and Guo & Finlay (1991) call it a *two-to-one* merging. The process is not completed by the last section shown (which is the exit section of the channel) but we can see that significant distortion of the cells involved occurs and that a slight adjustment in the position of all neighbouring pairs takes place. The resulting flow has a low wavenumber and is itself unstable to the Eckhaus instability that will tend to increase the spanwise wavenumber. Figure 12 shows a *two-to-three* splitting. It takes place at $t = 508$ halfway through the span of the curved channel. A stagnation point ($v = w = 0$) is formed in a downwash plane and as it moves towards the inner wall two new cells are formed. This process has a left–right mirror symmetry with respect to the new radial upwash plane created, and it produces a similar cell distortion and spanwise adjustment as in the opposite event.

### 5.1. *Eckhaus resonant mechanism and defect-mediated turbulence*

Defects propagate in space and time. The multiplication of defects in time is initially slow but becomes faster as time progresses. In figure 13 we show isolines of $u'$ in the same cross-section ($\theta = 2.915$) at several instants of time. Five, six or seven pairs may coexist in the cross-section at any given time. Vortices may remain aligned for several units of time (of the order of 100 s in physical time for experiments in air) early on, when a large degree of mirror symmetry about radial upwash planes is still present, and readjust their positions rapidly once merging or splitting takes place. This is in agreement with the observations of Ligrani & Niver (1988) who describe splitting of vortices and wavenumber readjustment to take place in less than 1 s. For $t > 600$ defects start breaking symmetries and decorrelating patterns. This is due to the interaction of defects, and it is illustrated in figure 14. The structures shown are strikingly similar to those observed in near-wall turbulent boundary layers (see for example figure 12 in Johansson, Alfredsson & Kim 1991). Large regions of positive streamwise perturbation velocity are shown next to regions of thin negative perturbation, and considerable spanwise movement (due to pairing and generation of streaky structures) is present. Johansson *et al.* (1991) pointed out that the development of asymmetry in the spanwise direction is a dominating feature in the evolution of near-wall structures in turbulent shear flows. The same consideration applies to the present flow. The complex structures produced are a consequence of the continuous chaotic forcing imposed; it is the unsteadiness of the forcing which is fundamental for the dynamics of the defects, rather than its origin. It is expected that the same qualitative pattern evolution would have taken place if a different fluctuating inlet perturbation had been applied.

Apart from qualitative similarities, we can scale the various dimensions of the observed structures in 'wall units' (by using a value of the streamwise wall shear stress averaged over the last thirty units of length in $R\theta$ and over the whole spanwise length) and we recover dimensions typical of turbulent boundary layers (see e.g. Cantwell 1981). The spanwise length of the domain covers a distance of 610 wall units, and since

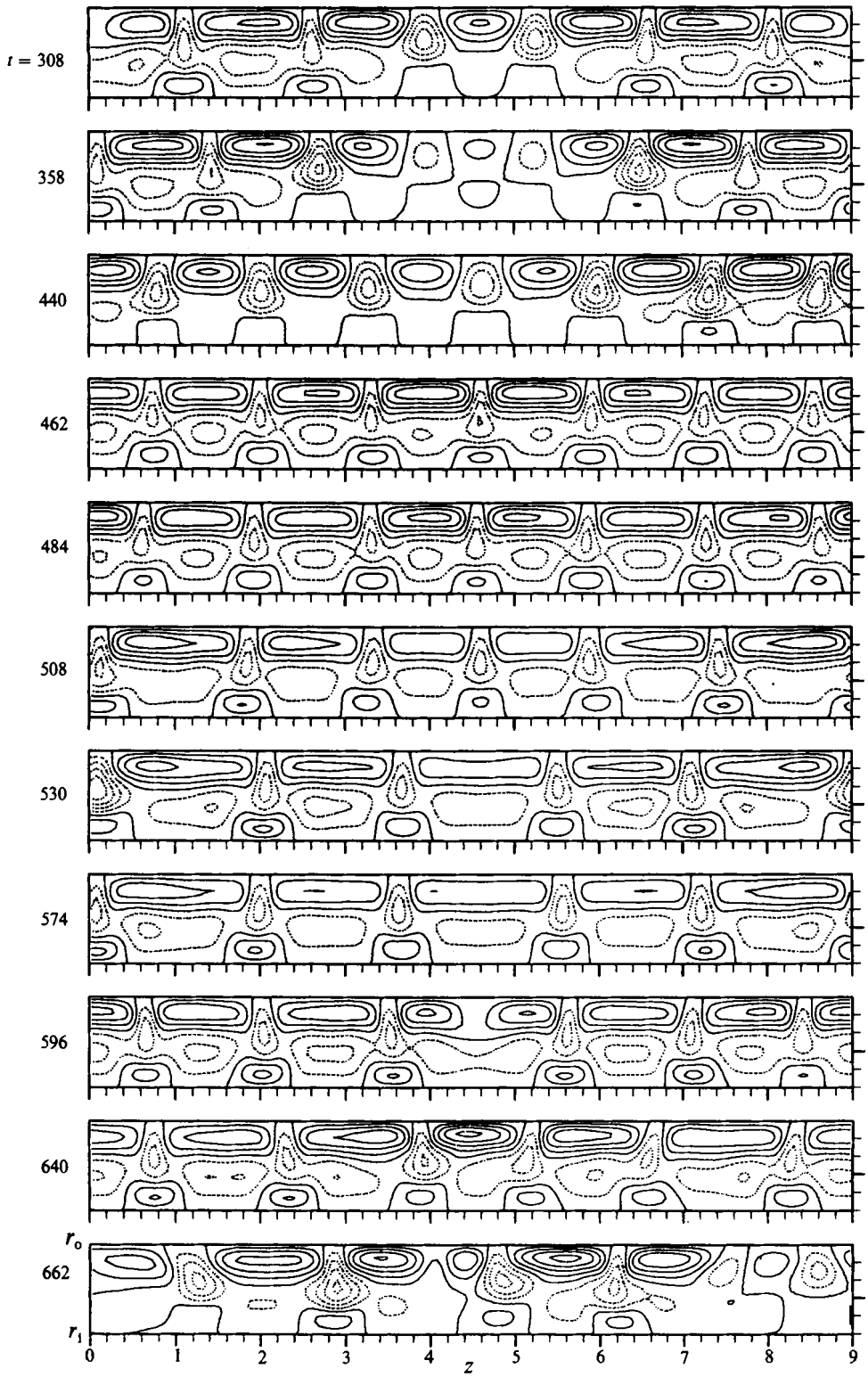


FIGURE 13. Streamwise perturbation velocity in the cross-section at $\theta = 2.915$ at 11 different instants in time. Isoline increment is 0.15.

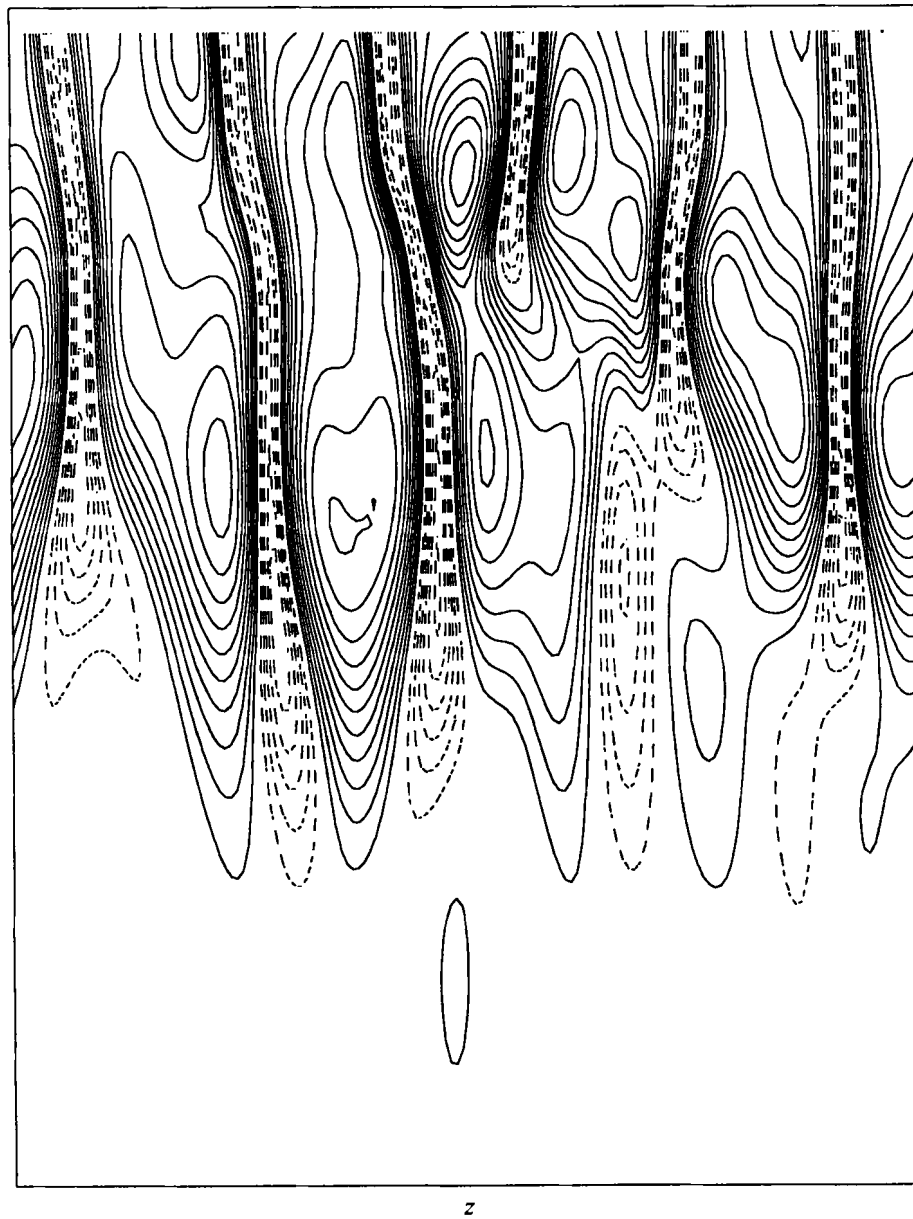


FIGURE 14. Streamwise perturbation velocity at $t = 644$ in an $(R\theta, z)$-plane, 9.4 viscous units of length away from the outer wall. Isoline increment is 0.05. The horizontal scale is stretched by 4.5.

between five and seven vortex pairs are present at any given time, typical spanwise spacings between the streaky structures found vary from 87 to 122 wall units. Streamwise lengths of the vortices range from a few hundred wall units to some thousands (although the upper limit is not identifiable because of the limited length of the computational domain). The main difference from coherent structures in turbulent boundary layers lies in the fact that the present vortices occupy the whole channel cross-section and are not concentrated towards a wall. After the vortices are formed near the concave (unstable) surface and move away from the wall with increasing $\theta$ (in a process that resembles an *ejection*), they eventually 'feel' the presence of the inner

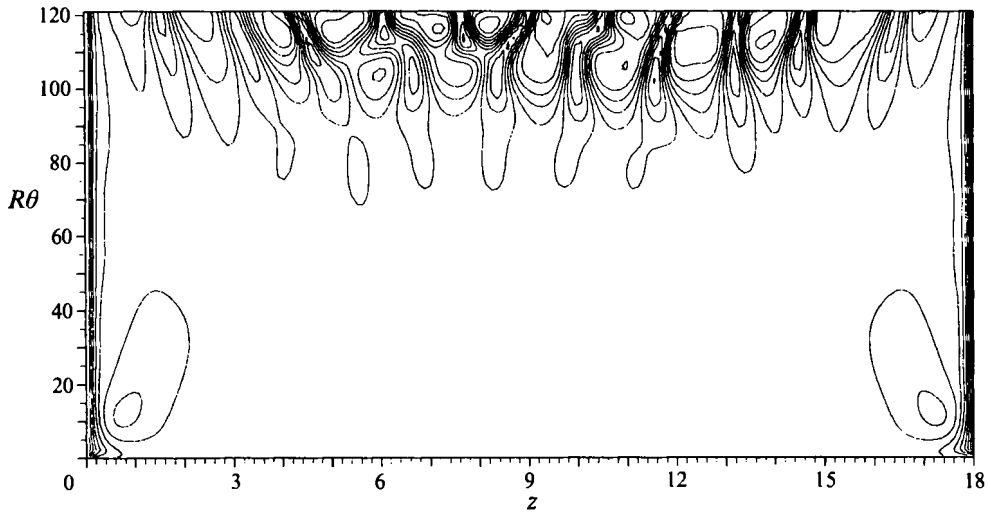


FIGURE 15. Isolines of $u$ in an $(R\theta, z)$-plane. Spacing is 0.1.

wall and react accordingly. This is the main difference between the present problem and the Görtler problem, where the vortices are not bound by two walls in the normal direction. In the case at hand the centre of the vortices is approximately halfway across the channel in the normal direction, which translates to about 34 wall units. According to Cantwell (1981) the centre of the streamwise vortices in turbulent boundary layers is between $10\nu/u_\tau$ and $25\nu/u_\tau$ where we denote by $u_\tau$ the friction velocity and by $\nu$ the viscosity. The difference could possibly be explained by the fact that the inner wall in the Dean problem limits the growth of the vortical structure between two closely spaced walls, whereas in a turbulent boundary layer tiny longitudinal vortices are continuously created in the sublayer, grow downstream to a critical size and are convected away by the free stream.

Finally, it is relevant to comment on the effect of sidewalls. A further simulation has been carried out for a channel of spanwise width equal to eighteen, but with no-slip solid boundaries at $z = 0$, 18. The number and distribution of grid points, initial and boundary conditions are the same as used so far in this section. In figure 15 isolines of streamwise velocity are shown at a time far enough away from the initial transient. Note the following: the flow is time-dependent and a sequence of merging and splitting processes occurs towards the exit of the channel, giving rise to uncorrelated patterns of low- and high-speed streaks. The defects are responsible for loss of symmetry of vortex pairs (when the vortices seem to bend), whereas the sidewall-induced Ekman vortices for $0 \leqslant R\theta \leqslant 50$ remain stationary. The dynamics of the Dean vortices is again controlled by interaction mechanisms, as in the spanwise-periodic case. This shows that sidewalls, although constraining the flow, do not stabilize it.

## 6. High-Reynolds-number steady flow

When the Reynolds number is sufficiently large, a secondary instability, in the form of high-frequency short-wavelength travelling waves ('twists'), is reported to occur. The onset of the instability as a function of the Reynolds number, at fixed curvature ratio, varies according to the type of investigation (numerical or experimental) and the length of the experimental domain. The theoretical threshold according to the linear stability analysis of Finlay *et al.* (1987, 1988) is $Re = 1.92Re_c$ at $\gamma = 0.975$. The basic

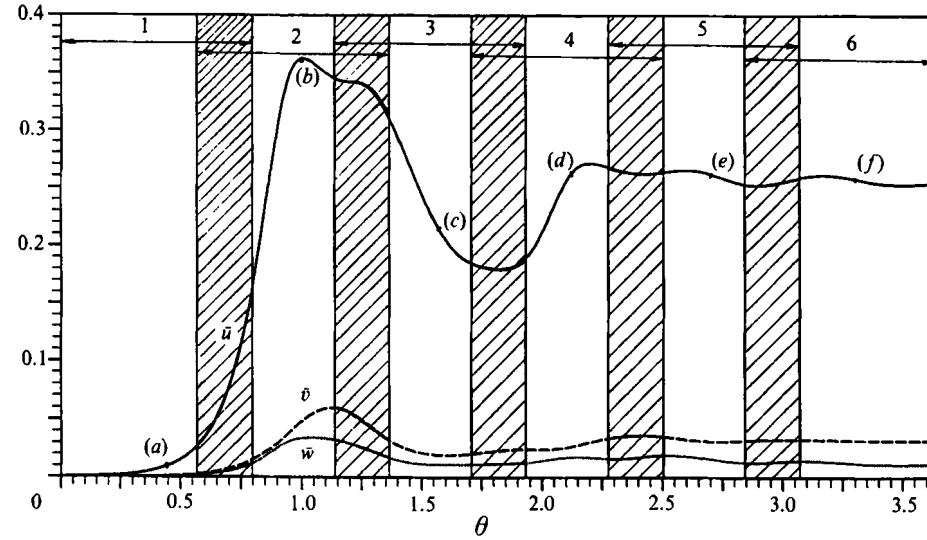


FIGURE 16. Average perturbation values of $u$, $v$, $w$ as a function of $\theta$. The six computational domains are indicated by the numbers 1–6, and the shaded regions are the regions of overlap between neighbouring computational domains.

flow they considered was a parallel flow computed with a temporally developing Navier–Stokes solver. The experiments by Kelleher *et al.* (1980) indicate an approximate onset at a value of $Re$ larger than $3Re_c$ in a channel of angular opening equal to $\pi$ and $\gamma = 0.979$. Matsson & Alfredsson (1992) consider a longer channel ($1.5\pi$) with $\gamma = 0.974$, so that twists develop earlier (at $Re \approx 2.8Re_c$).

The only spatially developing simulation of Dean flow in a parameter space for which the secondary instability could exist, has been carried out by Matsson *et al.* (1991) for $Re = 1455$ ($Re/Re_c = 6.47$) in a channel of angular extent equal to 1.75 and $\gamma = 0.974$. They provided comparisons between experimental and computational results on three different cross-sections that showed very good agreement between individual vortex pairs. However, that simulation fails to capture the correct temporal and streamwise spatial scales of the motion because of insufficient resolution in $\theta$. For a spatial simulation to resolve the whole flow properly from the inception of the Dean vortices past the onset of the streamwise wave (which has wavelength approximately equal to the width of the channel) requires a very high number of grid points in the streamwise direction. We have chosen to carry out such a simulation in a multiblock fashion. The technique used also provides some indirect arguments that reassure us as to the validity of the outflow boundary condition used. The complete computational domain has an angular extent equal to 3.64. Such a domain is divided into six partially overlapping subdomains as shown in figure 16, with Dirichlet inlet conditions applied at the inlet of each subdomain (and obtained, except for the first block, from the domain upstream) and convective outflow conditions applied at the exit boundary of each subdomain. The inlet condition on the first subdomain is CCPF. In the spanwise direction periodic conditions have been taken, with a spanwise length based on the average spanwise wavenumber found near the onset of the secondary instability in the experiments of Matsson & Alfredsson (1992); i.e. from their figure 15 one can find an average wavenumber $\beta = 5.80$. The cross-sectional grid has $30^2$ points (uniformly distributed in $z$ and smoothly concentrated near the walls in $r$), whereas each subdomain has 160 uniformly spaced nodes in $\theta$. The time step for the simulation is

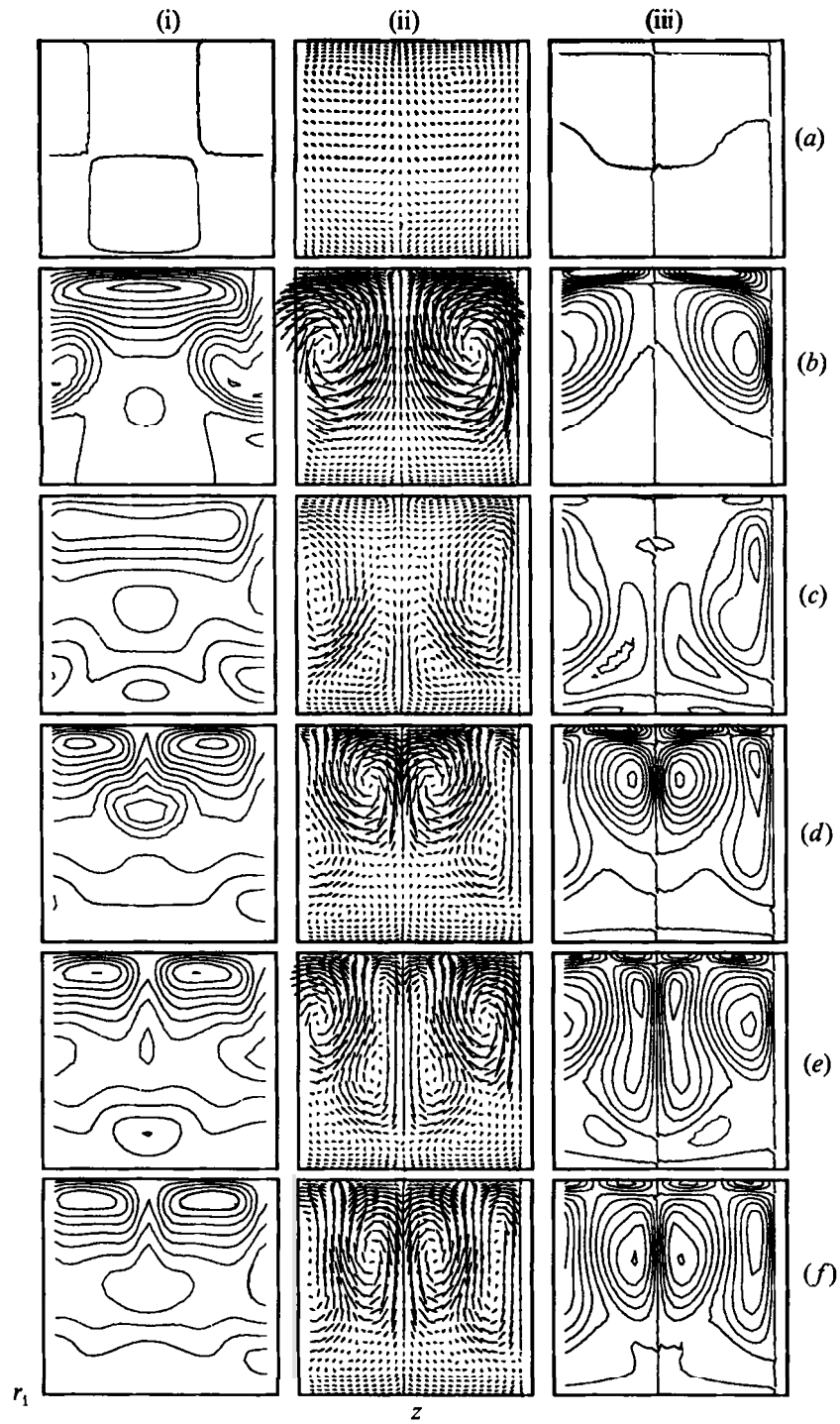


FIGURE 17. Streamwise perturbation velocity (i), secondary velocity vectors (ii) and streamwise vorticity (iii) for the six points (*a*)–(*f*) shown in figure 16. Isolines spacing is 0.15 on $u'$ and 0.2 on the streamwise vorticity. Zero contour lines are included.

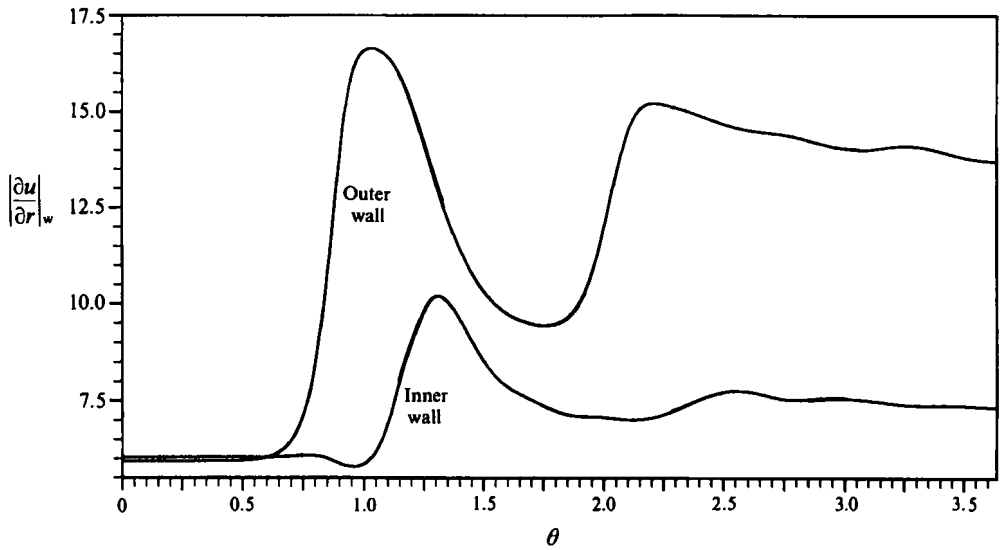


FIGURE 18. Wall shear stress on concave and convex boundaries as a function of $\theta$.

0.05 and four internal iterations are performed at each step. This is such that about four time steps are needed for an average fluid structure travelling in $\theta$ at the bulk speed to be convected across one control volume. The Reynolds number is taken to be equal to 1500 ($= 6.67Re_c$).

The results are displayed in figures 16–18. Figure 16 shows the spatial evolution of the average pertubation velocities. All perturbation velocities increase to a maximum value until $\theta \approx 1$. Here, the negative streamwise perturbation velocity (shown in figure 17) has a pear-like shape in the cross-section, whereas the positive streamwise perturbation velocity is elongated and concentrated towards the outer surface. As $\bar{u}$ decreases a splitting starts ($\theta > 1.25$) from the convex wall. The beginning of the formation of a new vortex pair at $r_i$ coincides with a maximum of wall stress on the convex surface. As the splitting progresses the new pair moves towards the outer wall and the shear stress on the inner wall decreases. The formation of a vortex pair near the inner wall has also been reported by Finlay *et al.* (1987). Vortices generated at convex walls by centrifugal forces can be expected when the velocity distribution at the wall is non-monotonic, as in the case of a wall jet (Floryan 1991). The appearance of a new vortex pair contributes to a new increase of $\bar{u}$ towards the approximately constant value of 0.25. Values of $\bar{v}$ and $\bar{w}$ are about one order of magnitude smaller than $\bar{u}$. Concerning the flow field, it is noteworthy that the two pairs of vortices coexisting in the cross-section oscillate (along $\theta$, not in time) in the normal direction until their centres are approximately 0.38 units of length from the concave wall (see (*f*) in figures 16 and 17). Measured in wall units (by using the spanwise-averaged shear stress on the concave wall) this is equal to approximately 55. The average spanwise spacing is of 78 wall units at point (*f*) in figures 16 and 17, whereas at (*b*) (where a vortex doubling is incipient) the spanwise spacing is 170. The spacings between vortices are in the range of those found for coherent structures in turbulent boundary layers.

It is important to point out that the flow field is stationary. This indicates, again, that merging and splitting of vortices are inherently steady events, as found in the detailed measurements of Matsson & Alfredsson (1992). Secondly, it indicates that the amplification of naturally occurring disturbances in a simulation (round-off errors) is too slow for the secondary instability to appear. To compute numerically a secondary

wavy instability with a spatial model one would need to introduce inlet perturbations of amplitudes typical of those encountered in experiments. The form of the perturbations should ideally be provided by the eigenfunctions of a secondary stability analysis. Some work along these lines has been undertaken by Le Cunff & Bottaro (1992).

These considerations lead us to the so-called *receptivity problem*, i.e. which eigenmodes will grow from background/environmental disturbances or, inversely, which background disturbances are responsible for flow phenomena observed experimentally.

The following scenario emerges.

(*a*) If the vortices are triggered by stationary disturbances (such as vortex generators or naturally occurring non-uniformities present in an experimental apparatus) they lock into place and grow downstream. Eventually they might merge steadily with neighbouring pairs or a new pair may form in the gap between two pairs. This is the case of the experiments of Matsson & Alfredsson (1992) and Bottaro *et al.* (1991) and it is attested to, in particular, by the fact that stationary non-uniformities at the inlet of their channel are responsible for (i) vortices that are always at the same spanwise positions at different Reynolds numbers, and (ii) events (in particular merging) that occur at the same spanwise locations at different Reynolds numbers. In the Görtler problem a similar situation may occur (Bippes 1978; T. Maxworthy 1990, personal communication).

(*b*) If low-amplitude fluctuating disturbances are present in the approaching flow the vortices are not locked into place and may seem to wander throughout the cross-section because of repetitive merging and splitting processes. Such an eventuality has been discussed theoretically by Guo & Finlay (1991) through a linear stability analysis; however, it should be remarked that the open nature of the flow and its receptivity characteristics cannot be completely accounted for in a stability analysis which considers a fully developed basic flow. Recent work by Y. Guo & W. H. Finlay (1992, personal communication) focuses on the Eckhaus stability of the spatially developing flow. Repetitive merging and splitting events have been reported by Ito (communicated to Floryan 1991, p. 266) for the Görtler problem. Some video sequences showing continuous interactions of Görtler vortices have been realized by Peerhossaini & Wesfreid (see also their related article, 1988). In the Dean problem a repetitive sequence of merging and splitting processes have been discovered by Ligrani & Niver (1988).

(*c*) A secondary instability in the form of streamwise travelling waves (Matsson & Alfredsson 1990) might be triggered above a critical Reynolds number when small perturbations in the incoming flow can be amplified. Disturbances of sufficient amplitude are typically and inherently present in most experimental apparatuses. In a temporally developing simulation perturbations may propagate and amplify continuously through the periodic boundary. In the present spatially developing simulations a secondary instability was not detected for a Reynolds number as high as $6.67Re_c$ because of the very slow initial amplification of background disturbances.

## 7. Summary

The flow in a curved channel has been examined through three-dimensional spatially developing simulations. Although temporal simulations may provide qualitative information on several flow phenomena, it is clear that the open and convective nature of the flow is properly represented only through a spatial approach. Furthermore, it is

important to consider channels of large-aspect-ratio cross-section to allow vortex pairs to adjust their spanwise positions freely. The simulations performed show an excellent agreement with linear stability results up to fairly high disturbance values and a very good agreement with experimental data in the nonlinear regime. By adopting the spatial approach we have found that merging and splitting phenomena are inherently steady and take place over several streamwise units of length; in a temporal approach interactions of these kinds appear to be always unsteady. A continuous and unsteady sequence of interaction processes between neighbouring vortex pairs may take place if the inlet flow is randomly perturbed in time with infinitesimal spanwise disturbances (Guo & Finlay 1991). This process produces structures which closely resemble coherent structures in turbulent boundary layers. As in turbulent wall flows (Johansson *et al.* 1991) an essential feature of longitudinal vortices is their spanwise movement. Similar spanwise shifts has been observed by Aubry *et al.* (1988) in their truncated simulations of the wall region of a turbulent boundary layer. The evolution of defects is probably one fundamental element of the breakdown process of longitudinal vortices and features of the flow described here are very close to those described by, among others, Coullet & Lega (1988), Coullet *et al.* (1989) and Bensimon *et al.* (1990).

The study of the spatial development of Dean vortex flow has revealed several interesting aspects that might have a bearing on more complex flow situations. In particular, because of the similarities between the present structures and those found in transitional and turbulent wall flows, ideas of direct applicability to flow management (riblets, LEBUs, etc.) might arise and be tested.

I would like to acknowledge Professor I. L. Ryhming for his support and encouragement, Professor P. H. Alfredsson, Mr O. J. E. Matsson, Professor T. Maxworthy and Professor A. Zebib for several interesting discussions. Mr Matsson provided the linear stability results displayed in figure 6. Some of the work has been performed during several visits to the Department of Mechanics/Fluid Physics of the Royal Institute of Technology in Stockholm. Their financial support is gratefully acknowledged, as is the support provided by Cray Research, through a University R & D Grant. The computations have been carried out on the Cray-2 of the Swiss Federal Institute of Technology, Lausanne.

## REFERENCES

ALFREDSSON, P. H. & PERSSON, H. 1989 Instabilities in channel flow with system rotation. *J. Fluid Mech.* **202**, 543.

AUBRY, N., HOLMES, P., LUMLEY, J. L. & STONE, E. 1988 The dynamics of coherent structures in the wall region of a turbulent boundary layer. *J. Fluid Mech.* **192**, 115.

BENNETT, J. & HALL, P. 1988 On the secondary instability of Taylor–Görtler vortices to Tollmien–Schlichting waves in fully developed flows. *J. Fluid Mech.* **186**, 445.

BENSIMON, D., KOLODNER, P., SURKO, C. M., WILLIAMS, H. & CROQUETTE, V. 1990 Competing and coexisting dynamical states of travelling-wave convection in an annulus. *J. Fluid Mech.* **217**, 441.

BIPPES, H. 1978 Experimental study of the laminar-turbulent transition of a concave wall in a parallel flow. *NASA TM* 75243.

BOTTARO, A. 1990 Note on open boundary conditions for elliptic flows. *Numer. Heat Transfer* B **18**, 243.

BOTTARO, A., MATSSON, O. J. E. & ALFREDSSON, P. H. 1991 Numerical and experimental results for developing curved channel flow. *Phys. Fluids* A **3**, 1473.

BROWAND, F. K. & PROST-DOMASKY, S. A. 1990 A technique for acoustic excitation of separated shear flows: preliminary results. In *Nonlinear Interaction Effects and Chaotic Motion* (ed. M. M. Reischman, M. P. Paidoussis & R. J. Hansen), vol. 7, p. 171. ASME.

BUELL, J. C. & HUERRE, P. 1988 Inflow/outflow boundary conditions and global dynamics of spatial mixing layers. *Stanford U./NASA Ames Rep.* CTR-S88, p. 19.

CANTWELL, B. J. 1981 Organized motion in turbulent flow. *Ann. Rev. Fluid Mech.* **13**, 457.

CHEN, C. C., LABHABI, A., CHANG, H.-C. & KELLY, R. E. 1991 Spanwise pairing of finite-amplitude longitudinal vortex rolls in inclined free-convection boundary layers. *J. Fluid Mech.* **231**, 73.

COULLET, P., GIL, L. & LEGA, J. 1989 Defect-mediated turbulence. *Phys. Rev. Lett.* **62**, 1619.

COULLET, P. & LEGA, J. 1988 Defect-mediated turbulence in wave patterns. *Europhys. Lett.* **7**, 511.

DANABASOGLU, G., BIRINGEN, S. & STREET, C. L. 1989 Numerical simulation of spatially-evolving instability. In *Instability and Transition*, Vol. II (ed. M. Y. Hussaini & R. G. Voigt), p. 394. Springer.

DEAN, W. R. 1928 Fluid motion in a curved channel. *Proc. R. Soc. Lond.* A **121**, 402.

FINLAY, W. H., KELLER, J. B. & FERZIGER, J. H. 1987 Instability and transition in curved channel flow. *Rep.* TF-30. Dept. of Mechanical Engineering, Stanford University.

FINLAY, W. H., KELLER, J. B. & FERZIGER, J. H. 1988 Instability and transition in curved channel flow. *J. Fluid Mech.* **194**, 417.

FINLAY, W. H. & NANDAKUMAR, K. 1990 Onset of two-dimensional cellular flow in finite curved channels of large aspect ratio. *Phys. Fluids* A **2**, 1163.

FLORYAN, J. M. 1991 On the Görtler instability of boundary layers. *Prog. Aerospace Sci.* **28**, 235.

GUO, Y. & FINLAY, W. H. 1991 Splitting, merging and wavelength selection of vortices in curved and/or rotating channel flow due to Eckhaus instability. *J. Fluid Mech.* **228**, 661.

HUERRE, P. & MONKEWITZ, P. A. 1990 Local and global instabilities in spatially developing flows. *Ann. Rev. Fluid Mech.* **22**, 473.

IKEDA, E. & MAXWORTHY, T. 1990 A note on the effects of polymer additives on the formation of Goertler vortices in an unsteady flow. *Phys. Fluids* A **10**, 1903.

JOHANSSON, A. V., ALFREDSSON, P. H. & KIM, J. 1991 Evolution and dynamics of shear-layer structures in near-wall turbulence. *J. Fluid Mech.* **224**, 579.

KELLEHER, M. D., FLENTIE, D. L. & MCKEE, R. J. 1980 An experimental study of the secondary flow in a curved rectangular channel. *Trans. ASME* I: *J. Fluid Engng* **102**, 92.

LE CUNFF, C. & BOTTARO, A. 1992 Linear stability of shear profiles and relation to the secondary instability of the Dean flow. *Phys. Fluids* A (Submitted).

LIGRANI, P. M. & NIVER, R. D. 1988 Flow visualization of Dean vortices in a curved channel with 40 to 1 aspect ratio. *Phys. Fluids* **31**, 3605.

LIU, W. & DOMARADZKI, J. 1990 Direct numerical simulation of transition to turbulence in Görtler flow. *AIAA* 90-0114.

LOWERY, P. S. & REYNOLDS, W. C. 1986 Numerical simulation of a spatially-developing, forced, plane mixing layer. *Rep.* TF-26. Dept. of Mechanical Engineering, Stanford University.

MARX, Y. P. 1991 A numerical method for the solution of the incompressible Navier–Stokes equations. *Rep.* T-91-3. IMHEF-DME, Swiss Federal Institute of Technology, Lausanne.

MATSSON, O. J. E., BOTTARO, A. & ALFREDSSON, P. H. 1991 Transition to turbulence in curved channel flow. In *Eighth Symp. on Turbulent Shear Flows, Sept. 9–11, 1911, Münich, Germany*, Paper 18-2.

MATSSON, O. J. E. & ALFREDSSON, P. H. 1990 Curvature- and rotation-induced instabilities in channel flow. *J. Fluid Mech.* **210**, 537.

MATSSON, O. J. E. & ALFREDSSON, P. H. 1992 Experiments on instabilities in curved channel flow. *Phys. Fluids* A **4**, 1666.

MUTABAZI, I., HEGSETH, J. J., ANDERECK, C. D. & WESFREID, J. E. 1990 Spatiotemporal pattern modulations in the Taylor–Dean system. *Phys. Rev. Lett.* **64**, 1729.

PATANKAR, S. V. 1980 *Numerical Heat Transfer and Fluid Flow*. McGraw-Hill.

PAULEY, L. L., MOIN, P. & REYNOLDS, W. C. 1990 The structure of two-dimensional separation. *J. Fluid Mech.* **220**, 397.

PEERHOSSAINI, H. & WESFREID, J. E. 1988 On the inner structure of streamwise Görtler rolls. *Intl J. Heat Fluid Flow* **9**, 12.

RAVI SANKAR, S., NANDAKUMAR, K. & MASLIYAH, J. H. 1988 Oscillatory flows in coiled square ducts. *Phys. Fluids* **31**, 1348.

SABRY, A. S. & LIU, J. T. C. 1991 Longitudinal vorticity elements in boundary layers: nonlinear development from initial Görtler vortices as a prototype problem. *J. Fluid Mech.* **231**, 615.

STUART, J. T. & DIPRIMA, R. C. 1978 The Eckhaus and Benjamin–Feir resonance mechanisms. *Proc. R. Soc. Lond.* A **362**, 27.

SWEARINGEN, J. D. & BLACKWELDER, R. J. 1987 The growth and breakdown of streamwise vortices in the presence of a wall. *J. Fluid Mech.* **182**, 255.

TAKEDA, A., KOBASHI, K. & FISCHER, W. E. 1990 Observation of the transient behaviour of Taylor vortex flow between rotating concentric cylinders after sudden start. *Exps. Fluids* **9**, 317.

THANGAM, S. & HUR, N. 1990 Fully developed flow in rectangular ducts. *J. Fluid Mech.* **217**, 421.

WINTERS, K. H. 1987 A bifurcation study of laminar flow in a curved tube of rectangular cross-section. *J. Fluid Mech.* **180**, 343.

YANG, K.-S. & KIM, J. 1991 Numerical investigation of instability and transition in rotating plane Poiseuille flow. *Phys. Fluids* A **4**, 633.

YEE, H. C. & SWEBY, P. K. 1992 On reliability of the time-dependent approach to obtaining steady-state numerical solutions. In *Proc. Ninth GAMM-Conf. on Numerical Methods in Fluid Mechanics* (ed. J. B. Vos, A. Rizzi & I. L. Ryhming), NNFM vol. 35, p. 512. Vieweg.